

Gravitational form factors of the proton in the improved holographic QCD model

Antti Hippeläinen,^a Niko Jokela,^a and Matti Järvinen^{b,c,d}

^a*Department of Physics and Helsinki Institute of Physics,
P.O. Box 64, FI-00014, University of Helsinki, Finland*

^b*Institute of Theoretical Physics, Chinese Academy of Sciences, Beijing 100190, China*

^c*Asia Pacific Center for Theoretical Physics, Department of Physics
Pohang 37673, Republic of Korea*

^d*Pohang University of Science and Technology,
Pohang 37673, Republic of Korea*

E-mail: antti.hippelainen@helsinki.fi, niko.jokela@helsinki.fi,
mattijarvinen@itp.ac.cn

ABSTRACT: We compute the gluonic contribution to the gravitational form factors of the proton using the improved holographic QCD model, in which the proton is described in terms of bulk Dirac fermions. Model parameters are constrained using lattice and phenomenological input, allowing us to obtain estimates for the gravitational form factors and to compare them with results from other approaches. The resulting $\mathcal{D}(t)$ form factor is found to exhibit an infrared pole in our framework. Using the extracted form factors, we analyze mechanical properties of the proton, including pressure and shear distributions. We obtain estimates of $\rho_{\text{mech}} = 0.95$ fm and $\rho_{\text{mass}} = 0.61$ fm for the mechanical and the mass radii of the proton, respectively, which are similar to values in other nonperturbative studies.

Contents

1	Introduction	3
2	Holographic model	4
2.1	Bulk gravity background	5
2.2	Fluctuations of bulk gravitational fields	6
2.3	Modeling the proton	7
3	Gravitational form factors	11
3.1	Holographic analysis	11
3.2	Fitting the model parameters to data	16
3.3	Prediction for $\mathcal{D}(t)$	17
4	Mechanical structure	19
4.1	Pressure and shear force distributions of a proton	20
4.2	Proton radius	22
5	Conclusions and outlook	25
A	Details on the computation of the form factors	27
A.1	Varying the fermion action	27
A.2	Restoring parity	29
B	Asymptotic solutions	31
B.1	IR asymptotics of the background	31
B.2	Near-boundary asymptotics of the background	32
B.3	Near-boundary asymptotics of the fermion wave functions	33
C	Mechanical consistency	34

1 Introduction

Probing the structure of the proton in the strongly coupled regime of quantum chromodynamics (QCD) remains a challenging problem. While the proton contains three valence quarks, its full structure involves a complex interplay of gluons and sea quarks that is still not fully understood.

The internal structure of the proton will be explored in unprecedented detail at the upcoming Electron-Ion Collider [1]. For the first time, spin-polarized beams of protons will be used, allowing for precision studies of spin-dependent properties and offering new insights into the long-standing proton spin puzzle [2]. Earlier experiments, such as HERA [3], have also contributed significantly to our understanding of proton structure.

The experimental studies of the proton focus on deep inelastic scattering (DIS) experiments. In DIS, a lepton, typically an electron, scatters off a hadron such as a proton, thereby probing its internal constituents [4]. In inclusive DIS, the hadronic final state is not fully reconstructed. Hard exclusive scattering processes, in which the proton remains intact and all final-state particles are detected, can provide complementary information to DIS and are sensitive to detailed aspects of the internal structure of the proton [5].

A key theoretical challenge is to access nonperturbative features of hadronic structure. While lattice QCD provides a first-principles nonperturbative approach, extracting spatially resolved and dynamical hadronic observables remains technically demanding, motivating the exploration of complementary theoretical frameworks. Holographic QCD models, inspired by the string/gravity correspondence, provide such a framework for this purpose. These models allow for a dual gravitational description of strongly coupled gauge theories, offering semi-quantitative predictions for observables that are otherwise difficult to compute. Over the past two decades, holography has been successfully applied to a wide range of problems in QCD-like theories, including hadron spectra, thermodynamics, and transport [6].

In this work, we study the gravitational form factors (GFFs) of the proton using a holographic approach. These form factors, $\mathcal{A}, \mathcal{B}, \mathcal{D}$, are defined through matrix elements of the energy-momentum tensor $T^{\mu\nu}(x)$ in a proton state [7, 8],

$$\langle p_2, s_2 | T^{\mu\nu}(x) | p_1, s_1 \rangle = \bar{u}(p_2, s_2) \left(\mathcal{A}(t) \frac{P^{\{\mu\gamma^\nu\}}}{2} + \mathcal{B}(t) \frac{i P^{\{\mu\sigma^\nu\}\alpha} k_\alpha}{4m_N} + \mathcal{D}(t) \frac{k^\mu k^\nu - \eta^{\mu\nu} k^2}{4m_N} \right) u(p_1, s_1) e^{ik \cdot x}, \quad (1.1)$$

where p_1 (p_2) and s_1 (s_2) are the on-shell momentum and spin of the incoming (outgoing) proton. For most of the work, we keep the spin indices implicit. Additionally, $t = k^2 \equiv -K^2$ with $k = p_2 - p_1$ being the exchanged momentum, bracketed indices $\mu, \nu, \alpha, \dots = 0, 1, 2, 3$ are symmetrized as $a^{\{\mu b^\nu\}} = (a^\mu b^\nu + a^\nu b^\mu)$, m_N is the mass of the proton, $P = (p_1 + p_2)/2$, and $\sigma^{\mu\nu} = \frac{i}{2}[\gamma^\mu, \gamma^\nu]$. The sign convention for η is mostly minus.

The gravitational form factors encode information about the distribution of energy, momentum, and internal forces inside the proton. These mechanical properties of the proton are not directly accessible experimentally and are currently inferred only through

model-dependent analyses of exclusive scattering data, or via lattice analysis. This motivates complementary non-perturbative theoretical approaches that can provide internally consistent predictions for these quantities. To this end, previous holographic studies of GFFs for nucleons and mesons include [8–15]; see also [16] for an early review of holographic form factors. In particular, the D-term or druck term, defined as the value of $\mathcal{D}(t)$ in the forward limit $t = 0$, remains poorly understood and has recently begun to attract interest also within the holographic community [11, 13].

In this work we focus only on the gluonic contribution to the form factors. We work with the improved holographic QCD (IHQCD) model [17–19], a holographic description of pure Yang–Mills theory that provides a phenomenologically realistic background geometry and has been successfully applied to a wide range of hadronic and thermodynamic observables. The background geometry is obtained by solving the five-dimensional gravitational equations of motion derived from the bulk action. The proton is modeled through a pair of bulk Dirac spinors. Matrix elements of the energy-momentum tensor are obtained via the holographic dictionary from the couplings induced by diffeomorphism invariance of the spinor action, allowing us to extract the GFFs of the proton. From these, we compute several quantities related to hadronic structure, including the gluonic $\mathcal{D}(t)$ form factor and mechanical properties of the proton.

The free parameters of the model are fixed by fitting the form factor $\mathcal{A}(t)$ to two sets of lattice data [20, 21], after which the form factor $\mathcal{D}(t)$ is determined without further adjustment. Away from the momentum-transfer threshold $t = 0$, the resulting $\mathcal{D}(t)$ shows a behavior comparable to that found in other theoretical analyses, while having an infrared (IR) pole in the present framework. Using the extracted form factors, we compute radial pressure and shear distributions inside the proton and compare them to existing theoretical and lattice-based studies. Finally, the proton radii obtained in our model are $\rho_{\text{mech}} = 0.95$ fm and $\rho_{\text{mass}} = 0.61$ fm.

The paper is organized as follows. In Section 2, we present the holographic model used to describe the background geometry and external sources. In Section 3, we compute the relevant couplings and extract the gravitational form factors. In Section 4, we analyze the mechanical structure of the proton implied by these form factors and compare our results to other theoretical approaches. We conclude in Section 5. Technical details are provided in Appendices A–C.

2 Holographic model

The five-dimensional gravitational model we work with is IHQCD [18, 19], a string-inspired model for pure glue Yang–Mills theory. Apart from the five-dimensional metric, which, as usual, is dual to the energy-momentum tensor in field theory, the model contains a dynamical dilaton field Φ . This field is interpreted to be dual to the $\text{Tr } G_{\mu\nu} G^{\mu\nu}$ operator where G is the field strength tensor of gluons and the trace is over color indices. Therefore, the dictionary of the model includes duals for the most important operators at weak coupling, *i.e.*, the ultraviolet (UV) marginal operators of the theory.

The action of IHQCD reads

$$S_{\text{IHQCD}} = -M_P^3 N_c^2 \int d^5 x \sqrt{-\det g} \left[\mathcal{R} - \frac{4}{3} (\partial \Phi)^2 - V(\Phi) \right] + 2M_P^3 N_c^2 \int_{\partial} d^4 x \sqrt{-\det h} \mathcal{K} , \quad (2.1)$$

where M_P is the Planck mass, N_c is the number of colors, \mathcal{R} is the Ricci scalar, h is the induced metric on the four-dimensional boundary manifold, and \mathcal{K} is the extrinsic curvature. The multiplier $M_P^3 N_c^2$ is related to the five-dimensional Newton constant as $G = 1/(16\pi M_P^3 N_c^2)$. The last term in (2.1) is the Gibbons–Hawking boundary term, which is needed to make the variational problem well defined. However, it does not play a further role in the analysis that follows.

In addition, $V(\Phi)$ is the dilaton potential, which holographically implements the renormalization group (RG) flow in the model. We use the dilaton potential from [22]:

$$V(\lambda) = 12 + V_1 \lambda + V_2 \frac{\lambda^2}{1 + \frac{\alpha_\lambda \lambda}{\lambda_0}} + 3V_{\text{IR}} e^{-\frac{\lambda_0}{\alpha_\lambda \lambda}} \frac{\lambda^{4/3}}{4\pi^{8/3}} \sqrt{\log \left(1 + \frac{\alpha_\lambda \lambda}{\lambda_0} \right)} \quad (2.2)$$

$$V_1 = \frac{44}{9\pi^2} , \quad V_2 = \frac{4619}{3888\pi^4} , \quad \lambda_0 = 8\pi^2 ,$$

where $\lambda = e^\Phi$. This form is designed to reproduce the correct UV and IR behavior of Yang–Mills theory [18, 19]. In particular, it matches the pure $SU(N_c)$ Yang–Mills β -function up to two-loop order in the UV, while yielding linear confinement in the IR. A detailed discussion of the construction and properties of the model can be found in [17].

The fit parameters in (2.2) take the values $\alpha_\lambda = 2.833$ and $V_{\text{IR}} = 7.231$. These were fixed in [22] by fitting the mass spectrum of light mesons, including radially excited states with masses up to approximately 2 GeV, in an extended version of the model that also incorporates quark degrees of freedom. The coefficients V_1 and V_2 are fixed by the UV matching to the Yang–Mills β -function.

Apart from the parameters of the potential and the five-dimensional Planck scale M_P , the model contains one additional dynamical parameter, namely the energy scale Λ that sets the overall scale of the background solutions.

2.1 Bulk gravity background

In order to solve the background metric in this model, we adopt the *Ansatz*

$$ds^2 = -e^{2A(r)} \eta_{MN} dx^M dx^N = e^{2A(r)} (-dt^2 + d\mathbf{x}^2 + dr^2) , \quad (2.3)$$

where $M, N = 0, \dots, 4$, and $\eta_{MN} = \text{diag}(1, -1, -1, -1, -1)$. Because scalings of the space-time coordinates (along with a scaling of r) can be absorbed by shifts of $A(r)$, its holographic interpretation is the logarithm of the energy scale [23]. The r -dependence of this factor is such that it cuts spacetime off dynamically once one enters the deep IR region of large r , hence making this model a certain kind of a soft-wall model. In these coordinates the UV boundary is located at $r = 0$ and the geometry ends in an IR singularity at $r = \infty$.

Background fields are solved from Einstein equations for dilaton gravity. After inserting the *Ansatz* (2.3), these equations boil down to

$$9A'^2 + 3A'' = e^{2A}V(\Phi) \quad (2.4)$$

$$3A'^2 - 3A'' = \frac{4}{3}(\Phi')^2, \quad (2.5)$$

where we suppressed the dependence of A and Φ on the holographic coordinate r , so that a prime denotes a derivative with respect to r . We follow similar notation for scalar functions throughout the text, unless writing the coordinate dependence explicitly is required for clarity. The IR and UV asymptotics of the geometry are presented explicitly in Appendix B, and in particular they give an explicit definition for the energy scale Λ of the background.

2.2 Fluctuations of bulk gravitational fields

The low-energy spectrum of the Yang–Mills theory contains scalar (spin zero) and tensor (spin two) glueball states. Through the holographic dictionary, these states can be studied in the dual picture by studying the linearized fluctuations of the metric and the dilaton around the gravity background. A complete analysis of linear gravity perturbations in Einstein-dilaton gravity can be found in [24]; here we will only discuss the details relevant for the current article.

After including generic scalar and tensor fluctuations, the metric can be written as

$$ds^2 = e^{2A(r)} [-(\eta_{\mu\nu} + 2h\eta_{\mu\nu} - 2\partial_\mu\partial_\nu E - 2h_{\mu\nu}^{TT})dx^\mu dx^\nu + 2\partial_\mu W dr dx^\mu + (1 + 2h_r)dr^2], \quad (2.6)$$

where $\eta_{\mu\nu} = \text{diag}(1, -1, -1, -1)$. The scalar fluctuation wave functions¹ $h(x, r)$, $E(x, r)$, $W(x, r)$, and $h_r(x, r)$, as well as the tensor fluctuation wave functions $h_{\mu\nu}^{TT}(x, r)$ are infinitesimal. Here TT stands for transverse and traceless, *i.e.*, $\partial^\mu h_{\mu\nu}^{TT} = \partial^\nu h_{\mu\nu}^{TT} = h_{\mu}^{TT\mu} = 0$. The linear perturbation of the dilaton Φ about the background value is denoted by $\varphi(x, r)$.

Infinitesimal scalar diffeomorphisms $r \mapsto r + \xi_r$, $x^\mu \mapsto x^\mu + \partial^\mu \xi$ act on the scalar perturbations as

$$\varphi \mapsto \varphi + \Phi' \xi_r, \quad h_r \mapsto h_r + A' \xi_r + \xi'_r, \quad h \mapsto h + A' \xi_r, \quad (2.7)$$

$$W \mapsto W + \xi_r + \xi', \quad E \mapsto E + \xi, \quad (2.8)$$

where we remind that the primes denote derivatives with respect to the holographic coordinate r . Consequently, we can define the following diffeomorphism covariant scalar variables

$$\mathcal{F} = h - \frac{A'}{\Phi'} \varphi, \quad \tilde{\mathcal{F}} = \frac{h}{A'} - W + E', \quad \mathcal{G} = h' - A' h_r + \frac{1}{3} \Phi' \varphi. \quad (2.9)$$

As it turns out, linearly perturbed Einstein equations imply that $\mathcal{G} = 0$ [24]. Moreover, \mathcal{F} and $\tilde{\mathcal{F}}$ are conjugate fields with relations

$$\tilde{\mathcal{F}}' + 3A' \tilde{\mathcal{F}} - \frac{1}{3} \left(\frac{\Phi'}{A'} \right)^2 \mathcal{F} = 0, \quad \partial_\mu \partial^\mu \tilde{\mathcal{F}} + \frac{1}{3} \left(\frac{\Phi'}{A'} \right)^2 \mathcal{F}' = 0. \quad (2.10)$$

¹For notational simplicity, we mark the coordinate dependence in the argument of all functions by x even though the wave functions may depend on the full coordinate vector x^μ , not only on its length.

The tensor mode satisfies

$$(h_{\mu\nu}^{TT})'' + 3A' (h_{\mu\nu}^{TT})' - \partial_\rho \partial^\rho h_{\mu\nu}^{TT} = 0. \quad (2.11)$$

As a consequence of the background depending only on the holographic coordinate r , the spacetime dependence of the equations becomes diagonal in Fourier space. To make this explicit, we write

$$\begin{aligned} \mathcal{F}(x, r) &= e^{-ik\cdot x} \hat{f}(k, r) \\ h_{\mu\nu}^{TT}(x, r) &= e^{-ik\cdot x} \epsilon_{\mu\nu}^{TT}(k) \hat{h}^{TT}(k, r), \end{aligned} \quad (2.12)$$

where the momentum space transverse-traceless projector satisfies $k^\mu \epsilon_{\mu\nu}^{TT} = k^\nu \epsilon_{\mu\nu}^{TT} = 0 = \epsilon_\mu^{TT\mu}$. Fluctuation equations (2.10) and (2.11) imply that the radial wave functions satisfy

$$\begin{aligned} (\partial_r^2 + 3A' \partial_r + k^2) \hat{h}^{TT}(k, r) &= 0 \\ \left(\partial_r^2 + \left(3A' + 2 \frac{X'}{X} \right) \partial_r + k^2 \right) \hat{f}(k, r) &= 0 \quad , \quad X \equiv \frac{\Phi'}{3A'} . \end{aligned} \quad (2.13)$$

Let \hat{f}_s and \hat{h}_s^{TT} denote the bulk-to-boundary propagator solutions. We define the boundary conditions for the propagators such that $\hat{h}_s^{TT}(k, r = 0) = \hat{f}_s(k, r = 0) = 1$, and impose regularity in the IR. Note that, as usual, the radial wave functions only depend on the momentum through $k^2 = k_\mu k^\mu$. Both of these fluctuation equations may be written in Schrödinger form where

$$-\left(\hat{h}^{TT}\right)'' + V_T \hat{h}^{TT} = -k^2 \hat{h}^{TT} , \quad -\hat{f}'' + V_S \hat{f} = -k^2 \hat{f} \quad (2.14)$$

with potentials

$$V_T = \frac{3}{4} A'^2 + \frac{3}{2} \frac{(e^A)''}{e^A} , \quad V_S = V_T + \frac{X''}{X} + 3A' \frac{X'}{X} . \quad (2.15)$$

The scalar potential term makes the glueball mass spectra non-degenerate. The spectrum of low-lying glueballs, which is obtained from the normalizable solutions to these equations, agrees well [25] with lattice data when using the potential (2.2), even though the potential was not fitted to Yang–Mills data but only to the experimental spectrum of full QCD.

2.3 Modeling the proton

In order to introduce an external proton in the model, we consider a simple approach where the proton is modeled as a fermionic field in the bulk. One is tempted to introduce the proton through a five-dimensional Dirac field in the gravity theory. However, this is problematic: a single five-dimensional Dirac fermion would, in general, model Weyl fermions at the boundary (see, *e.g.*, [26]), rather than Dirac fermions. In particular this means that the action for a five-dimensional Dirac field is not parity invariant. A parity-invariant model is obtained by considering a combination of two Dirac fields [27, 28]. Here, we will anyhow start with the action for a single field and discuss below how the model is made parity invariant.

The fermionic action reads

$$S_F = \mathcal{N} \int d^5x \sqrt{-\det g} \mathcal{L}_F + \mathcal{N} \int d^4x \sqrt{-\det g^{(4)}} \mathcal{L}_{UV} , \quad (2.16)$$

where \mathcal{N} is a normalization factor, and the Lagrangians are given by²

$$\mathcal{L}_F = e^{-\Phi} \left(\frac{i}{2} \bar{\Psi} e_B^N \gamma^B \partial_N \Psi - \frac{i}{2} (\partial_N \bar{\Psi}) e_B^N \gamma^B \Psi - \mathcal{V}_N(\Phi) \bar{\Psi} \Psi \right) \quad (2.17)$$

$$\mathcal{L}_{UV} = e^{-\Phi} (\bar{\Psi}_L \Psi_R + \bar{\Psi}_R \Psi_L) . \quad (2.18)$$

The first Lagrangian describes the dynamics of a Dirac fermion Ψ . The normalization factor \mathcal{N} is used as a fitting parameter. We also introduced the vielbeins e_B^N , with which the metric is represented as $g^{MN} = -e_A^M e_B^N \eta^{AB}$. Here the matrices having upper indices are the inverse metric and inverse of η . Since the metric is diagonal, vielbeins can be taken to be simply $e_B^N = e^{-A(r)} \delta_B^N$. The five-dimensional gamma-matrices are defined such that the first four matrices are the same as in the four-dimensional algebra, whereas the fifth matrix is $\gamma^r = -i\gamma^5$, with $\gamma^5 \equiv i\gamma^0\gamma^1\gamma^2\gamma^3$. They satisfy the algebra $\{\gamma^A, \gamma^B\} = 2\eta^{AB}$.

The second Lagrangian describes a four-dimensional boundary term, where $\Psi_L, \bar{\Psi}_L, \Psi_R$, and $\bar{\Psi}_R$ are the right- and left-handed parts of the full spinors $\Psi, \bar{\Psi}$ reduced to the boundary, $r = 0$. This boundary term is necessary to make the variational problem well-defined [27] but plays no further role in this article.

Let us then analyze the fermion spectrum. The equation of motion for fermions is

$$\left[ie_B^N \gamma^B D_N - \frac{i}{2} (\partial_N \Phi) e_B^N \gamma^B - \mathcal{V}_N(\Phi) \right] \Psi = 0 . \quad (2.19)$$

Here the covariant derivative is given by $D_N = \partial_N + \frac{1}{8} \omega_{NBC} [\gamma^B, \gamma^C]$, and ω_{NBC} is the spin-connection term. Its non-zero components are explicitly

$$\omega_{\mu r \nu} = -\omega_{\mu \nu r} = A'(r) \eta_{\mu \nu} . \quad (2.20)$$

As above, we write a plane-wave *Ansatz*

$$\Psi(x, r) = \tilde{\Psi}(p, r) e^{-ip \cdot x} . \quad (2.21)$$

The Fourier components can be decomposed as

$$\tilde{\Psi}(p, r) = \tilde{\Psi}_L(p, r) + \tilde{\Psi}_R(p, r) = e^{\frac{\Phi(r)}{2} - 2A(r)} [\psi_L(r) u_L(p) + \psi_R(r) u_R(p)] . \quad (2.22)$$

Here $\tilde{\Psi}_{L,R}(p, r) = (1 \mp \gamma^5) \tilde{\Psi}(p, r) / 2$, and $u_{L,R}(p) = (1 \mp \gamma^5) u(p) / 2$, with upper signs giving the conventions for left-handed spinors and $u(p)$ being the off-shell Dirac spinor. The radial wave functions $\psi_L(r)$ and $\psi_R(r)$ are scalar functions. We found it convenient to include the background dependent exponential factor in the last expression in (2.22).

²In principle, the derivatives in (2.17) should be promoted to covariant derivatives. In practice, however, the additional connection dependent terms cancel in our explicit computations, including the fluctuation analysis in Appendix A. This reflects the fact that the variations considered are generated by diffeomorphisms, for which the relevant combinations naturally assemble into Lie derivatives.

By using the fact that

$$\not{p} u_R(p) = m_n u_L(p) , \quad \not{p} u_L(p) = m_n u_R(p) , \quad (2.23)$$

with $m_n = \sqrt{p^2}$ for a bound state on-shell and solutions indexed as $n = 0, 1, 2, \dots$, separating the equation of motion (2.19) into left- and right-handed modes yields

$$-m_n \psi_L = \left[\frac{d}{dr} - e^A \mathcal{V}_N(\Phi) \right] \psi_R , \quad -m_n \psi_R = \left[-\frac{d}{dr} - e^A \mathcal{V}_N(\Phi) \right] \psi_L . \quad (2.24)$$

These coupled equations can in turn be written as second-order equations where the functions are decoupled:

$$\begin{aligned} m_n^2 \psi_R &= \left[-\frac{d^2}{dr^2} + \mathcal{V}_R \right] \psi_R , & \mathcal{V}_R &= e^{2A} \mathcal{V}_N(\Phi)^2 + \frac{d}{dr} (e^A \mathcal{V}_N(\Phi)) , \\ m_n^2 \psi_L &= \left[-\frac{d^2}{dr^2} + \mathcal{V}_L \right] \psi_L , & \mathcal{V}_L &= e^{2A} \mathcal{V}_N(\Phi)^2 - \frac{d}{dr} (e^A \mathcal{V}_N(\Phi)) . \end{aligned} \quad (2.25)$$

The bound state wave functions are normalized as

$$\int dr \psi_{L,R}^2(r) = 1 . \quad (2.26)$$

Normally, the mass spectrum is obtained from the normalized modes of the fluctuation equation. However, in the case of a bulk fermion, there are complications [29]. In general, there is no obvious way to pick a normalizable mode for fermions: the left- and right-handed wave functions are coupled through (2.24), which appears to prevent one from simultaneously requiring normalizability in both equations of (2.25).

This complication reflects the observation which we pointed out above: a single bulk Dirac fermion is not a good model for the proton, and only models half of the required degrees of freedom. That is, we need to choose whether the action (2.16) models the left- or right-handed component of the proton. We choose it to be the left-handed component, *i.e.*, that the spectrum is obtained by solving the Schrödinger problem for ψ_L in (2.25). Actually, for the specific potential $\mathcal{V}_N(\Phi)$ that we will be using here, this appears to be the only reasonable choice: as shown in Appendix B.3, the right-handed wave function ψ_R is UV-normalizable for all solutions, so requiring ψ_R to be normalizable instead would not lead to discrete spectrum.

Another way to see the interplay of the left- and right-handed functions is to study more closely their expansions near the boundary, which are solved explicitly in Appendix B.3. Recall that the standard picture in gauge/gravity duality is that each field has two independent solutions near the boundary, with the coefficient of the leading term being identified as the source (*e.g.*, a mass) and the coefficient of the subleading term is identified as the vacuum expectation value (VEV) of the dual operator. The coefficients are not linked by the equations of motion, but they become dependent after one imposes regularity (*e.g.*, finiteness of the action) in the IR. However, in the case of Dirac bulk fermion, the UV expansions only contain two independent coefficients even though there are two fields, ψ_L

and ψ_R . These two coefficients can be taken to be the leading coefficient of ψ_L and the leading coefficient of ψ_R . Then, we need to choose (see, *e.g.*, [27]), which of these coefficients is interpreted as the source and which is interpreted as the VEV. The above choice, *i.e.*, requiring that the mass spectrum is given by the Schrödinger equation for ψ_L , is equivalent to taking the leading coefficient of ψ_L as the source and the leading coefficient of ψ_R as the VEV.

We identify the proton as the lowest mode of the set of normalizable solutions, *i.e.*, we require the lowest mass (with $n = 0$) to be equal to the nucleon mass m_N ,

$$m_0 \equiv m_N . \quad (2.27)$$

The proton bulk eigenfunction is denoted by $\Psi_p^0(x, r)$, where the momentum of the proton state satisfies $p^2 = (m_0)^2$. It is understood that the wave functions ψ_L and ψ_R below are always specifically the eigensolutions of the proton state, and we do not indicate this explicitly for notational simplicity.

There is an undefined potential function in (2.17) which enters into the equations of motion of the proton. Following the philosophy in the IHQCD model [18, 19], we want to produce a mass spectrum for which squared masses are linear in the excitation number, $m_n^2 \sim n$, to reproduce standard Regge-like behavior. This is obtained by choosing the potential \mathcal{V}_N appropriately. The requirement translates into choosing $\mathcal{V}_N(\Phi)$ in (2.17) such that the left-handed Schrödinger potential \mathcal{V}_L evaluated on the gravity background grows as $\sim r^2$ in the IR. Given the IR asymptotics of the background in Appendix B, this boils down to the requirement

$$\mathcal{V}_N(\Phi) \sim e^{\frac{2}{3}\Phi} \Phi^{\frac{1}{4}} \quad (2.28)$$

as $\Phi \rightarrow \infty$. We choose a parametrization which satisfies this requirement and is smooth for all values of Φ ,

$$\mathcal{V}_N(\Phi) = v_N e^{\frac{2}{3}\Phi} (1 + \Phi^2)^{\frac{1}{8}} , \quad (2.29)$$

where v_N is a constant. Note that it can be matched with the proton mass, but this also requires fixing the overall energy scale, which amounts to determining the value of the parameter Λ defined in Appendix B.3. We will do this later when comparing the model to the data for the gravitational form factors.

As we pointed out above, the fermion action (2.17) cannot be made parity-invariant. Parity may be restored by adding another bulk Dirac fermion in the model, which is the chiral partner of the Ψ in (2.17). The action of the chiral partner is obtained from (2.17) by flipping the sign of γ^5 . This means that the γ -matrix in the holographic direction, γ^r , flips its sign, and left- and right-handed components are interchanged, *e.g.*, $\psi_L \leftrightarrow \psi_R$. The full action with parity restored is given explicitly in Appendix A.2, see Eq. (A.10).

In the action for the chiral partner, we take the leading coefficient in the UV expansion of the right-handed field (instead of the left-handed one) ψ_R to be the source, as required by parity covariance. However, note that the equations of motion for the chiral partner are obtained from (2.24) by also switching the labels L and R . As the switch happens both in the equations and in their boundary conditions, the mass levels remain unchanged.

3 Gravitational form factors

Having set the holographic model, we turn to identifying and computing the gravitational form factors. This requires us to fluctuate the fermionic action (2.17) with respect to the metric to extract the matrix element of the energy-momentum tensor with the holographic dictionary. From this matrix element we identify the form factors $\mathcal{A}(t)$ and $\mathcal{D}(t)$ present in our model. The remaining parameters are then fit into sets of recent lattice data, and results are compared across various studies.

3.1 Holographic analysis

In order to analyze the gravitational form factors of the proton in field theory via holography, we need to compute the matrix element $\langle p_2 | T^{\mu\nu} | p_1 \rangle$ in (1.1) using the holographic dictionary. The dictionary for the energy-momentum tensor is the usual: it is dual to the metric of the five-dimensional gravity theory. However, there are some complications about the proton state. First, as we discussed above, the proton is actually modeled through the sum over two five-dimensional Dirac fermions with opposite chiralities. Second, by using the usual definition of the dictionary in terms of generating functionals, it is straightforward to compute correlators of operators, but not scattering amplitudes with on-shell particles.

The first complication is handled by summing over the contributions from the Dirac fermions, see Appendix A.2 for details. In the main text, we will often only consider contributions from a single fermion for simplicity. As for the second complication, a well-known formalism exists. One may start by considering a three-point function with two insertions of a baryon operator \mathcal{O}_Ψ dual to Ψ and one insertion of $T_{\mu\nu}$. One then transforms the three point function to Fourier space, which introduces momenta for all three operators. Then one studies the limit where the baryon momenta become on-shell. By the Lehmann–Symanzik–Zimmermann (LSZ) reduction formula, the three-point function becomes, after removing divergences, proportional to the desired matrix element (in Fourier space). On the gravity side, an analogous reduction takes place [30]. Following the Gubser–Klebanov–Polyakov dictionary [31], the generating functional for correlators is obtained in terms of IR-regular fluctuation wave functions, *i.e.*, wave functions for which the fluctuated action is IR-finite, and which reduce to desired boundary values at the UV, which act as sources for the field theory operators. However, in the limit where the momentum of a fluctuation wave function becomes on-shell, the IR-regular wave function becomes ill-defined due to a presence of sourceless regular solutions corresponding to the bound states. In the case of Dirac fermions in the setup discussed above, these solutions are given by the normalizable solutions to the (left-handed) Schrödinger equation in (2.25). This means that as one approaches the on-shell value of the momentum, the fluctuation wave functions diverge. This divergence matches exactly the divergence of the correlator in field theory. Therefore, after applying the LSZ reduction, one recovers the gravity expression for the amplitude, where the fermion fluctuation wave functions are replaced by the coefficients of their divergent terms, *i.e.*, the sourceless normalizable bound state wave functions.

The variation with respect to the sources in the metric is done as usual. Varying the gravity action boils down to varying with respect to the sources for the dynamical

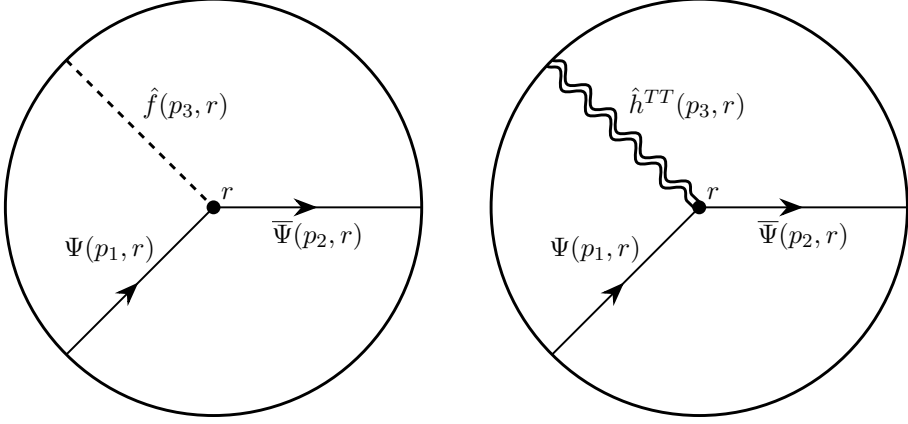


Figure 1. Two possible Witten diagrams for three-point functions including Dirac spinors.

fluctuations of the metric \mathcal{F} and $h_{\mu\nu}^{TT}$. To make the definition concrete, we choose a gauge where the fluctuations of the rr and $r\mu$ -components of the metric vanish, *i.e.*, use the diffeomorphism transformations in (2.7) and (2.8) to set $W = 0$ and $h_r = 0$. Then the fluctuations of the metric are contained in

$$ds^2 = e^{2A(r)} [-(\eta_{\mu\nu} + h_{\mu\nu})dx^\mu dx^\nu + dr^2] \quad (3.1)$$

$$h_{\mu\nu} = 2h\eta_{\mu\nu} - 2\partial_\mu\partial_\nu E - \partial_{\{\mu}V_{\nu\}}^T - 2h_{\mu\nu}^{TT}. \quad (3.2)$$

Here we also included the vectorial perturbation $V_\mu^T(x, r)$, where the superscript T indicates that the field is transverse, $\partial^\mu V_\mu^T = 0$. This field is in principle required in order to write a consistent variation formula for the energy-momentum tensor operator.³ However, the vectorial field is not a physical propagating mode and its bulk wave functions are trivial (r -independent), see, *e.g.*, [24]. It could still contribute to the matrix element $\langle p_2 | T^{\mu\nu} | p_1 \rangle$ which we want to compute, but as it turns out, it does not (see Appendix A.1). Therefore, we will not discuss the contribution from this field further. Given the above gauge choice, we may write the boundary condition involving the variation of the field theory metric $\delta\eta_{\mu\nu}(x)$, which couples to the energy-momentum tensor operator $T_{\mu\nu}$, as

$$h_{\mu\nu}(x, r = 0) = \delta\eta_{\mu\nu}(x). \quad (3.3)$$

In Fourier space, the evaluation of the three-point function therefore boils down to computing the Witten diagrams in Fig. 1, with the understanding that the fermion lines represent the on-shell normalizable fluctuation wave functions. The most nontrivial part of the Witten diagram is the vertex between the fermions and the metric fluctuations. This vertex is obtained from the fermion action (2.16). Note that since our setup does not have fermionic background, the contributions from this action start at second order in the fluctuations. The desired vertex is found from the third-order fluctuation term, which is

³By this we mean that there is no regular solution to the fluctuation equations satisfying the boundary condition (3.3) for any $\delta\eta_{\mu\nu}$, unless we also include the vectorial field.

obtained by fluctuating the metric in the Lagrangian (2.17) (see Appendix A.1 for details). A straightforward computation gives for this term⁴

$$S_F^{(3)} = \mathcal{N} \int d^5x \sqrt{-\det g} e^{-\Phi} \left[\frac{d\mathcal{V}_N(\Phi)}{d\Phi} \bar{\Psi} \Psi \mathcal{F} \frac{\Phi'}{A'} + \frac{i}{6} \frac{\Phi'^2}{A'^2} e^{-A} (\bar{\Psi}' \gamma^r \Psi - \bar{\Psi} \gamma^r \Psi') \mathcal{F} + \frac{i}{2} e^{-A} \partial_\mu (\bar{\Psi}' \gamma^\mu \Psi - \bar{\Psi} \gamma^\mu \Psi') \tilde{\mathcal{F}} + \frac{i}{2} e^{-A} (\partial^\mu \bar{\Psi} \gamma^\nu \Psi - \bar{\Psi} \gamma^\mu \partial^\nu \Psi) h_{\mu\nu}^{TT} \right], \quad (3.4)$$

where prime denotes a derivative with respect to the holographic coordinate r as before, and the gauge-invariant combinations of the fluctuation wave functions of the metric: \mathcal{F} , $\tilde{\mathcal{F}}$, and $h_{\mu\nu}^{TT}$ are defined in Section 2.2. Because the additional gauge-invariant wave function \mathcal{G} vanishes after imposing the Einstein equations, we have omitted the terms involving this field.

Taking into account the above considerations, we can finally write down the correspondence between the field theory amplitude and gravity action. We first define the on-shell vertex as

$$S_{F_{\text{o-s}}}(p_2, p_1)[\delta\eta_{\mu\nu}] = S_F^{(3)} \Big|_{\bar{\Psi}=\bar{\Psi}_{p_2}^0, \Psi=\Psi_{p_1}^0, h_{\mu\nu}|_{\text{bdry}}=\delta\eta_{\mu\nu}}, \quad (3.5)$$

where $S_F^{(3)}$ is given in (3.4), and the proton wave functions⁵ are as defined in Section 2.3. Note that this expression is a function of the proton momenta and a functional of the boundary variation $\delta\eta_{\mu\nu}$. The source of the dilaton variation φ is set to zero. The above discussion leads to the following identification

$$\int d^4x e^{ip\cdot x} \langle p_2 | T^{\mu\nu}(x) | p_1 \rangle = (2\pi)^4 \delta^{(4)}(p - p_1 + p_2) \langle p_2 | T^{\mu\nu}(0) | p_1 \rangle \propto \int d^4x e^{ip\cdot x} \frac{\delta S_{F_{\text{o-s}}}^{(3)}}{\delta(\delta\eta_{\mu\nu}(x))}. \quad (3.6)$$

Therefore taking the inverse Fourier transform gives simply

$$\langle p_2 | T^{\mu\nu}(x) | p_1 \rangle \propto \frac{\delta S_{F_{\text{o-s}}}^{(3)}}{\delta(\delta\eta_{\mu\nu}(x))}. \quad (3.7)$$

The proportionality coefficient, which arises from the holographic LSZ reduction, is not needed for our purposes: it turns out that it can be absorbed into other parameters of the setup.

In order to evaluate the functional derivative in (3.7), it is useful to compute the on-shell vertex (3.5) explicitly. We sketch here the main points, see Appendix A.2 for details.

⁴We do not attempt to keep track of boundary terms in this computation. As far as we can see, all boundary terms will eventually vanish after we insert the proton wave functions, thanks to their UV asymptotics, which are analyzed in Appendix B.

⁵To be precise, we need to insert the wave functions for both Dirac fermions that model the proton in a way which conserves parity, see Appendix A.2.

Using (3.2) and (3.3), we can solve the boundary values of the metric fluctuations

$$\begin{aligned}
h(x, r=0) &= \frac{1}{6}(\eta^{\mu\nu} - \partial^\mu \partial^\nu / \partial^2) \delta\eta_{\mu\nu}(x) \\
E(x, r=0) &= \frac{1}{6} \frac{1}{\partial^2} (\eta^{\mu\nu} - 4\partial^\mu \partial^\nu / \partial^2) \delta\eta_{\mu\nu}(x) \\
h_{\mu\nu}^{TT}(x, r=0) &= \left[-\frac{1}{2} (\delta_\mu^\alpha - \partial^\alpha \partial_\mu / \partial^2) (\delta_\nu^\beta - \partial^\beta \partial_\nu / \partial^2) \right. \\
&\quad \left. + \frac{1}{6} (\eta^{\alpha\beta} - \partial^\alpha \partial^\beta / \partial^2) (\eta_{\mu\nu} - \partial_\mu \partial_\nu / \partial^2) \right] \delta\eta_{\alpha\beta}(x) \\
&\equiv -\frac{1}{2} \varepsilon_{\mu\nu}^{TT, \alpha\beta} \delta\eta_{\alpha\beta}(x) ,
\end{aligned} \tag{3.8}$$

where the operator inverse $1/\partial^2$ is defined as

$$\frac{1}{\partial^2} f(x) \equiv \int \frac{d^4 p}{(2\pi)^4} e^{-ip \cdot x} \frac{1}{-p^2} \hat{f}(p) , \tag{3.9}$$

for any function f and its Fourier transform \hat{f} . Because we only turn on sources for the fluctuations of the metric and not for the dilaton, from (2.9) we see that the boundary values of the diffeomorphism invariant fluctuation \mathcal{F} and the scalar metric fluctuation h match,

$$h(x, r=0) = \mathcal{F}(x, r=0) . \tag{3.10}$$

Moreover, because the term involving $\tilde{\mathcal{F}}$ in (3.4) vanishes after we have inserted the solutions for the wavefunctions of the proton state (see Appendix A.2), we only need the solutions for the fluctuations \mathcal{F} and $h_{\mu\nu}^{TT}$. They may be written as

$$\begin{aligned}
\mathcal{F}(x, r) &= \int \frac{d^4 p}{(2\pi)^4} \hat{f}_s(p, r) e^{-ip \cdot x} \int d^4 y e^{ip \cdot y} h(y, r=0) \\
&= \int \frac{d^4 p}{(2\pi)^4} \hat{f}_s(p, r) e^{-ip \cdot x} \frac{1}{6} (\eta^{\mu\nu} - p^\mu p^\nu / p^2) \int d^4 y e^{ip \cdot y} \delta\eta_{\mu\nu}(y)
\end{aligned} \tag{3.11}$$

$$\begin{aligned}
h_{\mu\nu}^{TT}(x, r) &= \int \frac{d^4 p}{(2\pi)^4} \hat{h}_s^{TT}(p, r) e^{-ip \cdot x} \int d^4 y e^{ip \cdot y} h_{\mu\nu}^{TT}(y, r=0) \\
&= \int \frac{d^4 p}{(2\pi)^4} \hat{h}_s^{TT}(p, r) e^{-ip \cdot x} \left(-\frac{1}{2} \hat{\varepsilon}_{\mu\nu}^{TT, \alpha\beta}(p) \right) \int d^4 y e^{ip \cdot y} \delta\eta_{\alpha\beta}(y) ,
\end{aligned} \tag{3.12}$$

where

$$\hat{\varepsilon}_{\mu\nu}^{TT, \alpha\beta}(p) = (\delta_\mu^\alpha - p^\alpha p_\mu / p^2) (\delta_\nu^\beta - p^\beta p_\nu / p^2) - \frac{1}{3} (\eta^{\alpha\beta} - p^\alpha p^\beta / p^2) (\eta_{\mu\nu} - p_\mu p_\nu / p^2) . \tag{3.13}$$

Inserting these and the proton wavefunctions in (3.4) yields (see Appendix A.2)

$$\begin{aligned}
S_{F_{\text{o-s}}}^{(3)}(p_2, p_1)[\delta\eta_{\mu\nu}] &= \mathcal{N} \int dr \left[2 \frac{\Phi'}{A'} e^A \frac{d\mathcal{V}_N(\Phi)}{d\Phi} \bar{u}(p_2) \psi_L \psi_R u(p_1) \hat{f}_s(k, r) \frac{1}{6} (\eta^{\mu\nu} - k^\mu k^\nu / k^2) \right. \\
&\quad + \frac{2}{6} \left(\frac{\Phi'}{A'} \right)^2 \bar{u}(p_2) (\psi'_L \psi_R - \psi_L \psi'_R) u(p_1) \hat{f}_s(k, r) \frac{1}{6} (\eta^{\mu\nu} - k^\mu k^\nu / k^2) \\
&\quad \left. + (\psi_R^2 + \psi_L^2) \bar{u}(p_2) \frac{P^{\{\alpha\gamma\beta\}}}{2} u(p_1) \hat{h}_s^{TT}(k, r) \left(-\frac{1}{2} \hat{\epsilon}_{\alpha\beta}^{TT, \mu\nu}(k) \right) \right] \\
&\quad \times \int d^4y e^{ik\cdot y} \delta\eta_{\mu\nu}(y) ,
\end{aligned} \tag{3.14}$$

where $k = p_2 - p_1$.

Taking the functional derivative in (3.7) therefore gives

$$\begin{aligned}
\langle p_2 | T^{\mu\nu}(x) | p_1 \rangle &= \frac{2}{6} \tilde{\mathcal{N}} \int dr \frac{\Phi'}{A'} e^A \frac{d\mathcal{V}_N(\Phi)}{d\Phi} \psi_R \psi_L \hat{f}_s(k, r) \frac{1}{k^2} \bar{u}(p_2) (k^2 \eta^{\mu\nu} - k^\mu k^\nu) u(p_1) e^{ik\cdot x} \\
&\quad + \frac{2}{36} \tilde{\mathcal{N}} \int dr \left(\frac{\Phi'}{A'} \right)^2 (\psi_R \psi'_L - \psi'_R \psi_L) \hat{f}_s(k, r) \frac{1}{k^2} \bar{u}(p_2) (k^2 \eta^{\mu\nu} - k^\mu k^\nu) u(p_1) e^{ik\cdot x} \\
&\quad - \frac{1}{2} \tilde{\mathcal{N}} \int dr (\psi_R^2 + \psi_L^2) \hat{h}_s^{TT}(k, r) \bar{u}(p_2) \frac{P^{\{\mu\gamma\nu\}}}{2} u(p_1) e^{ik\cdot x} \\
&\quad + \frac{1}{6} \tilde{\mathcal{N}} \int dr (\psi_R^2 + \psi_L^2) \hat{h}_s^{TT}(k, r) \bar{u}(p_2) m_N \frac{1}{k^2} (k^2 \eta^{\mu\nu} - k^\mu k^\nu) u(p_1) e^{ik\cdot x} ,
\end{aligned} \tag{3.15}$$

where $k = p_2 - p_1$ and the dimensionless coefficient $\tilde{\mathcal{N}}$ is the product of \mathcal{N} and the dimensionful proportionality constant in the relation (3.7). Comparing with the decomposition of the matrix element,

$$\langle p_2 | T^{\mu\nu}(x) | p_1 \rangle = \bar{u}(p_2) \left(\mathcal{A}(t) \frac{P^{\{\mu\gamma\nu\}}}{2} + \mathcal{B}(t) \frac{i P^{\{\mu\sigma\nu\}} \alpha k_\alpha}{4m_N} + \mathcal{D}(t) \frac{k^\mu k^\nu - \eta^{\mu\nu} k^2}{4m_N} \right) u(p_1) e^{ik\cdot x} , \tag{3.16}$$

where the Mandelstam variable is defined as $t = k^2$, we may directly identify the form factors. Noting that there is no structure corresponding to \mathcal{B} it is identically zero, while the other two form factors read

$$\mathcal{A}(t) = -\frac{\tilde{\mathcal{N}}}{2} \int dr \hat{h}_s^{TT}(\sqrt{-t}, r) (\psi_R^2 + \psi_L^2) \tag{3.17}$$

$$\begin{aligned}
\mathcal{D}(t) &= -\frac{8m_N \tilde{\mathcal{N}}}{6t} \left[\frac{1}{2} m_N \int dr \hat{h}_s^{TT}(\sqrt{-t}, r) (\psi_R^2 + \psi_L^2) + \int dr \hat{f}_s(\sqrt{-t}, r) \right. \\
&\quad \left. \times \left(\left(\frac{\Phi'}{A'} \right) e^A \frac{d\mathcal{V}_N(\Phi)}{d\Phi} \psi_R \psi_L + \frac{1}{6} \left(\frac{\Phi'}{A'} \right)^2 (\psi_R \psi'_L - \psi'_R \psi_L) \right) \right] .
\end{aligned} \tag{3.18}$$

3.2 Fitting the model parameters to data

We first need to fix the remaining model parameters. There are three free parameters left, which are the overall normalization $\tilde{\mathcal{N}}$, the coefficient v_N multiplying the proton potential in (2.29), and the characteristic energy scale Λ .

In order to understand the fitting procedure, it is useful to analyze the units of energy in our setup. There are actually two natural ways to assign the units. They can be defined through the following transformations, which leave the action invariant (possibly up to an overall factor). The first one,

$$x^\mu \mapsto x^\mu/\Lambda_\ell, \quad r \mapsto r/\Lambda_\ell, \quad V(\Phi) \mapsto V(\Phi)\Lambda_\ell^2, \quad M_P \mapsto M_P\Lambda_\ell, \quad (3.19)$$

$$\mathcal{V}_N(\Phi) \mapsto \mathcal{V}_N(\Phi)\Lambda_\ell, \quad (3.20)$$

is perhaps the canonical choice. It leaves the components of the metric unchanged but alters the potentials V and \mathcal{V}_N . Therefore it also sets the units of the AdS radius, which is determined from the UV normalization of V (see Appendix B.3), to the inverse of energy as expected. We could also assign units to the fermionic field Ψ , but these are not needed for our purposes, and can be absorbed in the dimension of $\tilde{\mathcal{N}}$. The second one, is obtained by transforming the components of the metric instead, $g_{\mu\nu} \mapsto g_{\mu\nu}\Lambda_s^2$, or in terms of the scale factor A ,

$$x^\mu \mapsto x^\mu/\Lambda_s, \quad r \mapsto r/\Lambda_s, \quad A \mapsto A + \log \Lambda_s \quad (3.21)$$

with all other fields and parameters unchanged. That is, the potentials and the AdS radius are also unchanged and therefore counted as dimensionless. Note that the four-momenta transform as $k^\mu \mapsto k^\mu\Lambda_s$, and masses of bound states also transform linearly in Λ_s .

Since the line element is invariant under (3.21), it is immediate that the action is invariant. In particular, the transformation $e_B^N \mapsto e_B^N/\Lambda_s$ of the vielbein cancels the transformation of the derivative in the fermion action (2.17). This latter transformation may appear unnatural, since it does not respect the expected dimensions of the potentials and the AdS radius. However, the fact that the potentials are unchanged under this transformation also means that it is a symmetry of the solutions of the equation of motion. The parameter in the background solution which corresponds to this symmetry is the scale factor Λ . Therefore, when analyzing the solutions numerically, we can change the value of Λ through the symmetry (3.21). The freedom corresponding to the first transformation (3.19) is fixed by choosing the UV normalization of the potential $V(\Phi)$ such that the AdS radius ℓ equals one.

The basic idea of the fit is that the coefficient of the fermion potential, v_N , is determined by the proton mass, whereas $\tilde{\mathcal{N}}$ and Λ are determined by fitting data for the form factor $\mathcal{A}(t)$. Note that thanks to the symmetry (3.21), changing Λ corresponds to scaling the t -dependence of the form factors, while changing $\tilde{\mathcal{N}}$ changes the normalization, which makes fitting the form factor rather straightforward. However, note that the fits to the proton mass and the form factor are not independent: Since the proton mass changes under the symmetry (3.21) while the potential $\mathcal{V}_N(\Phi)$ does not, the fit is affected by the value of Λ . Conversely, the choice of the coefficient v_N affects the shape of the holographic result for

$\mathcal{A}(t)$ and therefore modifies the fit of the form factor. Therefore, we carry out the two fits iteratively until convergence is found.

We fit our form of $\mathcal{A}(t)$ to the lattice data for the gluonic contributions to $\mathcal{A}(t)$ obtained in [20, 21]. Only data for $\mathcal{A}(t)$ are used in the fit, since these are significantly more uniform than the currently available results for $\mathcal{D}(t)$. An additional motivation for this choice is that fixing $\mathcal{A}(t)$ allows remaining proton properties, which are determined through $\mathcal{D}(t)$, to be predicted within the model. Had $\mathcal{D}(t)$ been fitted directly instead, the resulting mechanical properties would largely be imposed by the fit itself rather than emerging as genuine model predictions. At each step of the iterative fitting procedure we do a least-squares fit of $\mathcal{A}(t)$ to the data [20, 21], taking into account the error estimates in the data.

We pick an initial value $v_N \approx 1$ and fit Λ repeatedly to lattice data using the proton mass and other parameters. This procedure converges quickly after only a few iterations and yields the parameters $v_N \approx 1.53$, $\tilde{N} \approx 0.503$, and $\Lambda \approx 24.7$ MeV. This sets $\mathcal{A}(0) \approx 0.503$, and as required, $m_N \approx 0.938$ GeV.

We then compare our fit to earlier studies. In many studies (*e.g.*, [10, 20, 21, 32]) one encounters so-called multipole fits for the form factor profiles. They are common mainly due to their reasonably good reproduction of results and analytic simplicity. They are of the form

$$\mathcal{A}_{\text{pol}}(t) = \frac{\mathcal{A}(0)}{\left(1 - \frac{t}{M_{\mathcal{A}}^2}\right)^{\alpha_{\mathcal{A}}}} , \quad (3.22)$$

where $M_{\mathcal{A}}$ is an energy scale and $\alpha_{\mathcal{A}}$ is an exponent which becomes relevant at high t . Similar profiles are encountered also for $\mathcal{D}_{\text{pol}}(t)$ with analogous parameters $\mathcal{D}(0)$, $M_{\mathcal{D}}$, and $\alpha_{\mathcal{D}}$. Common choices for the parameters α_i , with $i = \mathcal{A}$ or $i = \mathcal{D}$, are $\alpha_i = 2$ (dipole fit) and $\alpha_i = 3$ (tripole fit).

We also plot a parametrized form motivated by the soft-wall-based study of [10]. Choosing $\mathcal{A}(0) = 0.58$, $M_{\mathcal{A}} = 1.124$ GeV, and $\alpha_{\mathcal{A}} = 2$ yields a curve that matches the corresponding result shown there to good precision. For the lattice data of Hackett et al. [21], the form factor $\mathcal{A}_{\text{pol}}(t)$ has been fit with parameters $\mathcal{A}(0) = 0.501 \pm 0.027$, $M_{\mathcal{A}} = 1.262 \pm 0.018$ GeV, and $\alpha_{\mathcal{A}} = 2$. The $\mathcal{A}_{\text{pol}}(t)$ of Shanahan et al. from [20] has parameters $\mathcal{A}(0) = 0.58$, $M_{\mathcal{A}} = 1.13$ GeV, and $\alpha_{\mathcal{A}} = 2$.

We compare our lattice data-fit holographic profile of $\mathcal{A}(t)$ (black solid curve) to the multipole fits listed above in Fig. 2. The lattice data marked in green is from [20], and data marked in orange from [21]. Note that our IHQCD result is computed directly from the model rather than a dipole formula. The different fits of $\mathcal{A}(t)$ are comparable for a range of t -values, and our holographic numerical result overlaps with the lattice fit of Hackett et al. [21], in particular at small $|t|$.

3.3 Prediction for $\mathcal{D}(t)$

As one readily checks from (3.17), there are no parameters left to fit for $\mathcal{D}(t)$. We thus compare the results of the holographic form factor $\mathcal{D}(t)$, predicted by the lattice data fit of $\mathcal{A}(t)$, to lattice and phenomenological results (see Fig. 3).

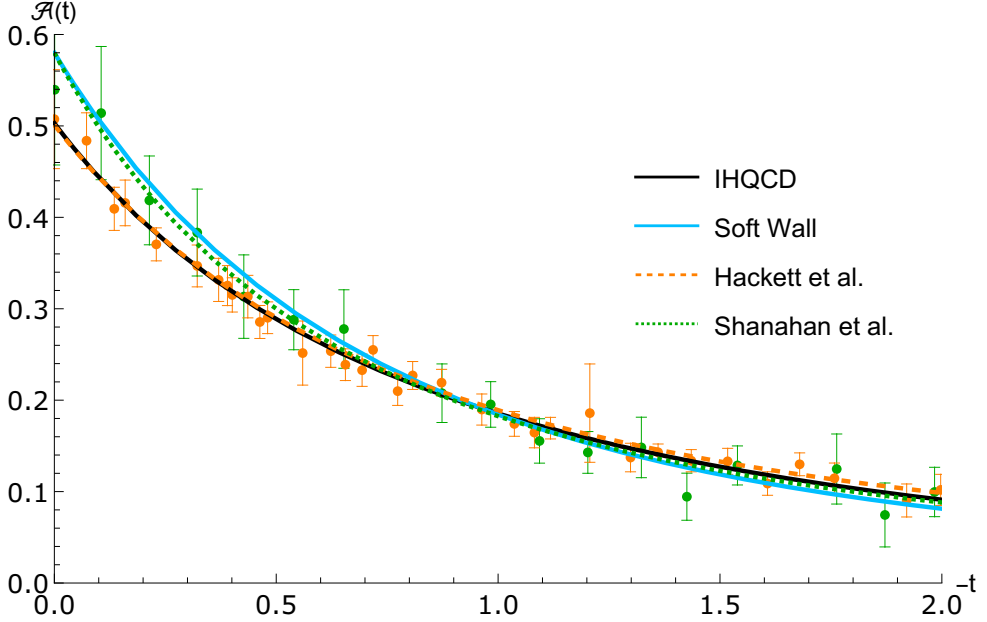


Figure 2. Results for the form factor $\mathcal{A}(t)$. Green data points and the green curve (Shanahan et al.) are based on lattice data from [20]. Orange data points and the orange curve (Hackett et al.) are based on lattice data from [21]. The soft-wall-based result is from [10]. The black solid curve is our fit.

The phenomenological curves shown in purple are obtained in [33] from analyses of DVCS data [32, 33], based on measurements by the CLAS Collaboration [34, 35]. Since DVCS observables receive contributions from both quark and gluon degrees of freedom, they therefore involve modeling assumptions about the relative quark and gluon contributions.

For the lattice data of Hackett et al. [21], the form factor $\mathcal{D}_{\text{pol}}(t)$ has been fit with parameters $\mathcal{D}(0) = -2.57 \pm 0.84$, $M_{\mathcal{D}} = 0.538 \pm 0.065$ GeV, and $\alpha_{\mathcal{D}} = 2$. The $\mathcal{D}(t)$ result by Shanahan et al. [36] has parameters $\mathcal{D}(0) = -7.08$, $M_{\mathcal{D}} = 0.763$ GeV, and $\alpha_{\mathcal{D}} = 3$. The fit to experimental DVCS data in Burkert et al. [33] has parameters $\mathcal{D}(0) = -1.47 \pm 0.06 \pm 0.14$, $M_{\mathcal{D}}^2 = 1.02 \pm 0.13 \pm 0.21$ GeV 2 , and $\alpha_{\mathcal{D}} = 2.76 \pm 0.23 \pm 0.48$. These results are compared to our holographic results (solid black curve).

There is considerable variation between different $\mathcal{D}(t)$ -profiles in Fig. 3. However, the error bars are also large, and the IHQCD results, the DVCS fit, and the lattice results of [21] are relatively close in the range where data is available.

Of special interest in many studies has been the D-term, *i.e.*, the value $\mathcal{D}(0)$ of the form factor at zero momentum transfer [7]. We find that the value for the D-term diverges in our model in the IR as $\mathcal{D} \propto \frac{m_N^2}{-t}$. However, this behavior does not necessarily indicate any inconsistency; as emphasized recently, such divergences can naturally arise. For example, for pions $\mathcal{D}(t)$ develops an infrared pole in the chiral limit [37, 38]. Moreover, $\mathcal{D}(t)$ diverges when coupled with QED [39]. However, the pole at $t = 0$ in the $\mathcal{D}(t)$ of our holographic model does not appear to be linked to a massless state. Nevertheless, as we show below, all physical observables related to the proton remain regular. Notice that the value derived

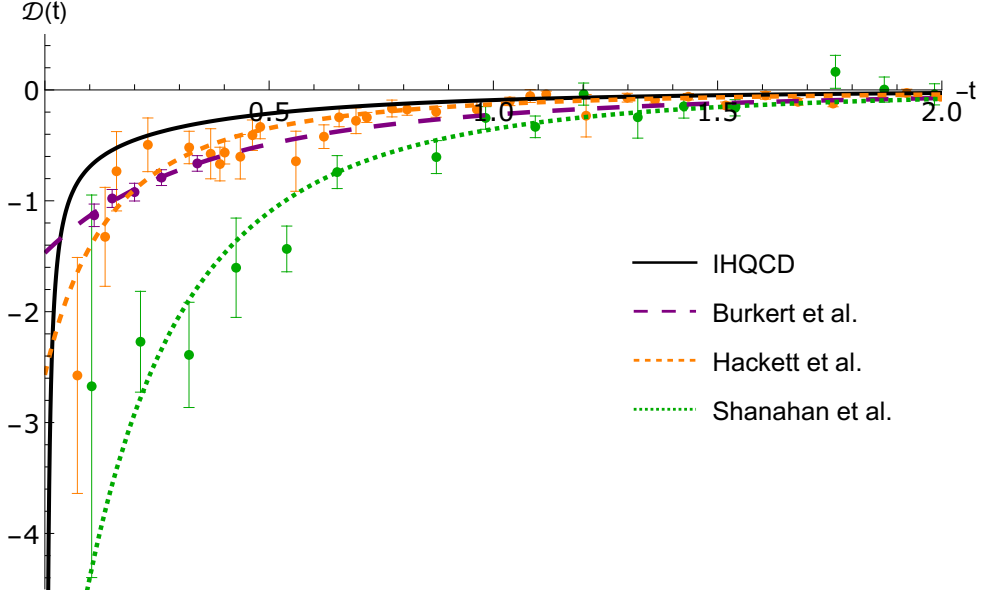


Figure 3. Our prediction (solid black curve) compared to various results for the form factor $\mathcal{D}(t)$. Green data points and the green curve (Shanahan et al.) are based on lattice data from [36], orange ones (Hackett et al.) are based on lattice data from [21], and the purple ones (Burkert et al.) are based on the fit of [33] to DVCS data from [34, 35]. Dashed curves are multipole fits (3.22) to the data points using the values given below this respective equation.

from the top-down holographic Witten–Sakai–Sugimoto model is finite, $\mathcal{D}(0) = -2.05$ [13].

Interestingly, we observe that while our D-term is divergent, the contributions from the two integrals in (3.18) numerically cancel within the accuracy of $\sim 5\%$. This cancellation does not seem to arise from any obvious symmetry in our setup. Thanks to the cancellation, the residue of the pole at $t = 0$ in the fit of Fig. 3 is suppressed, making a good description of the data possible.

4 Mechanical structure

In this section we present holographic results for the mechanical properties of the proton. By definition, gravitational form factors encode information about matrix elements of the energy-momentum tensor of the proton. In particular, the form factor $\mathcal{D}(t)$ is related to spatial deformations of the proton and provides access to its mechanical properties. These include quantities such as pressure and shear force distributions, as well as proton radii defined from moments of the corresponding distributions.

Such mechanical properties have been studied using lattice QCD [20, 21], phenomenological extractions based on DVCS data [32, 33], and holographic approaches [10]. In the case of experimental data, these quantities are obtained indirectly and necessarily rely on modeling assumptions and theoretical constraints, since pressure and shear distributions are not directly observable. It has been emphasized that present data alone are insufficient to determine mechanical properties of the proton in a model-independent manner, and that

phenomenological extractions necessarily involve assumptions about functional forms and extrapolations [40, 41]. Consistency conditions following from mechanical stability further constrain the allowed distributions, as reviewed in Appendix C.

4.1 Pressure and shear force distributions of a proton

The spatial components of the energy-momentum tensor T_{ij} can be decomposed using the pressure $p(\rho)$ and shear $s(\rho)$ profiles of the proton into a trace and traceless part [7]

$$T_{ij}(\rho) = p(\rho)\delta_{ij} + s(\rho)\left(\frac{\rho_i\rho_j}{\rho^2} - \frac{1}{3}\delta_{ij}\right), \quad (4.1)$$

where ρ is the position vector from the center of the proton, ρ_i are its components, and ρ denotes its length. These pressure and shear force distributions may be computed directly from the \mathcal{D} form factor. We obtain spatial information by transforming into coordinate space,

$$\tilde{\mathcal{D}}(\rho) = \int \frac{d^3K}{2m_N(2\pi)^3} e^{-i\mathbf{K}\cdot\rho} \mathcal{D}(-\mathbf{K}^2). \quad (4.2)$$

Then, the pressure and shear profiles can be expressed in terms of $\tilde{\mathcal{D}}(\rho)$ as [7]

$$p(\rho) = \frac{1}{3} \frac{1}{\rho^2} \frac{d}{d\rho} \left(\rho^2 \frac{d}{d\rho} \tilde{\mathcal{D}}(\rho) \right), \quad s(\rho) = -\frac{1}{2} \rho \frac{d}{d\rho} \left(\frac{1}{\rho} \frac{d}{d\rho} \tilde{\mathcal{D}}(\rho) \right). \quad (4.3)$$

Note that carrying out the transform in (4.2) requires the knowledge of $\mathcal{D}(t)$ at arbitrarily large $|t|$. However, it turns out to be challenging to compute $\mathcal{D}(t)$ numerically at large enough $|t|$ in our model. Therefore, we match the numerical result along its first two derivatives with an asymptotic expansion to $\mathcal{D}(t)$ at approximately $-t = 5$ GeV², and use the expansion to extrapolate to high $|t|$. We use the form $\mathcal{D}(t) = -\left(\frac{D_1}{t^3} + \frac{D_2}{t^5} + \frac{D_3}{t^7}\right)$ in the extrapolation, which agrees the asymptotic behavior predicted by QCD counting rules [42, 43]. The values of parameters obtained from matching are $D_1 \approx 0.357$, $D_2 \approx 0.337$, and $D_3 \approx -4.38$.

In Figs. 4 and 5 we compare the holographic result for the pressure and shear force distributions to two different lattice results (obtained from the tripole fit of [36], and the dipole fit of [21]) and the result obtained from dipole analysis of DVCS data [33]. The holographic results are similar to the DVCS fit and the recent lattice result of [21], while differing significantly from the earlier lattice result of [36].

As is also required by mechanical consistency, the pressure profiles are positive at low values of ρ . In all models, for ρ between 0.5 fm and 0.8 fm the pressure crosses from positive to negative values. The integral over $\rho^2 p(\rho)$ as is required for the stability of the nucleon, see Appendix C, or alternatively directly by analyzing (4.3).

For the shear force, our holographic results are again similar to the dipole fit result of [32] and the result of lattice analysis in [21], but significantly different from lattice result of [20]. The lattice result from the fit of [21] raises quicker than our prediction at low ρ , but its maximum is located at approximately the same radius as the maxima of the holographic result and the DVCS fit of Burkert et al. [32]. The behavior at low ρ is connected to the power with which $-\mathcal{D}(t)$ decays at high momentum transfer. The decay behavior based

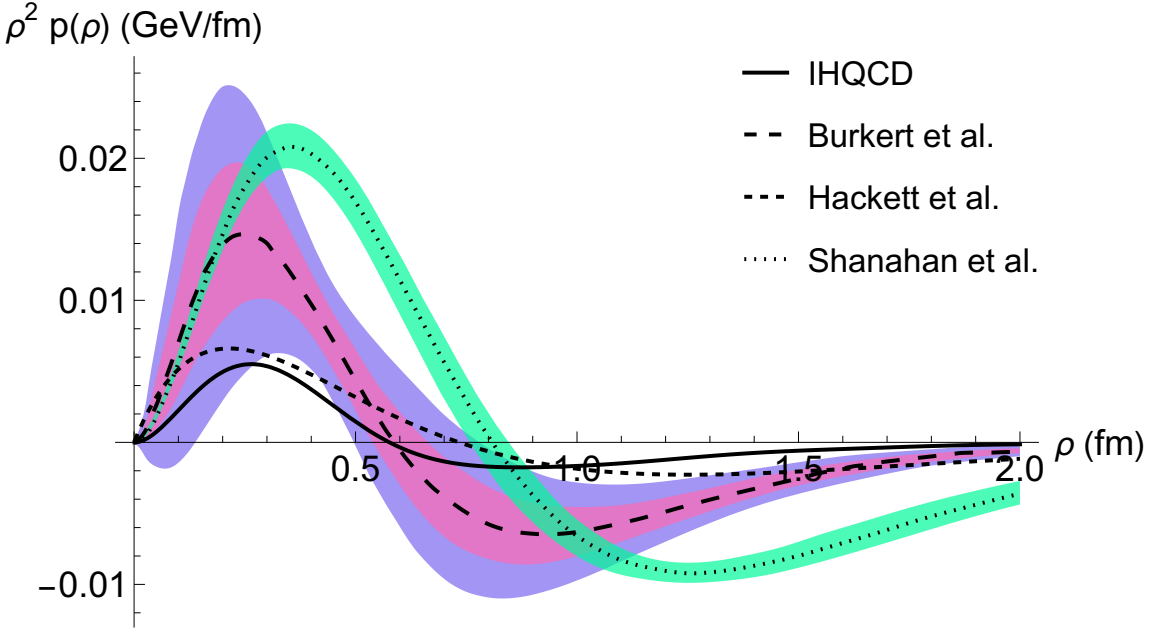


Figure 4. Pressure distributions (4.3) of a proton, as given by different models. The long-dashed black curve, as well as the violet and pink bands arise from a dipole fit analysis of DVCS data from Burkert et al., [32]. The violet band shows the error estimate of [32], compared to a future projection (pink band). The dotted curve with green error band is a lattice fit result taken from [36]. The result labeled Hackett et al. is computed by us from the form of $\mathcal{D}(t)$ given in [21].

on the multipole fit of [32] is approximately $\mathcal{D}(t) \sim 1/(-t)^3$, which again conforms with predictions of QCD counting rules [42, 43].

One may define tangential and normal forces acting inside a proton from the pressure and shear profiles [7]. They are defined with respect to a principal axis ρ , θ , or ϕ , and the sign of their value represents squeezing or stretching in this direction. By a classical analogy, multiplying a pressure by the area element allows us to compute forces acting inside a proton. The profiles can be computed from the decomposition of the spatial part of the energy momentum tensor (4.1). For example, projecting T^{ij} onto the radial unit vector $\hat{\rho}$ yields

$$p_\rho(\rho) \equiv \hat{\rho}^i T_{ij} \hat{\rho}^j = \frac{2}{3} s(\rho) + p(\rho) . \quad (4.4)$$

We similarly obtain the angular contribution,

$$p_\theta(\rho) = p_\phi(\rho) = -\frac{1}{3} s(\rho) + p(\rho) . \quad (4.5)$$

By angular isotropicity, $p_\theta = p_\phi$. We present visualizations of the normal and tangential pressure distributions for the four models in Figs. 6 and 7. By a classical analogy such pressures may be related to forces inside a proton. Hence, the magnitude of the normalized profiles describes the relative magnitudes of forces acting inside a proton.

The holographic result for the radial pressure profile is similar with the two lattice results, while the prediction for tangential pressures matches best with the DVCS fit. In

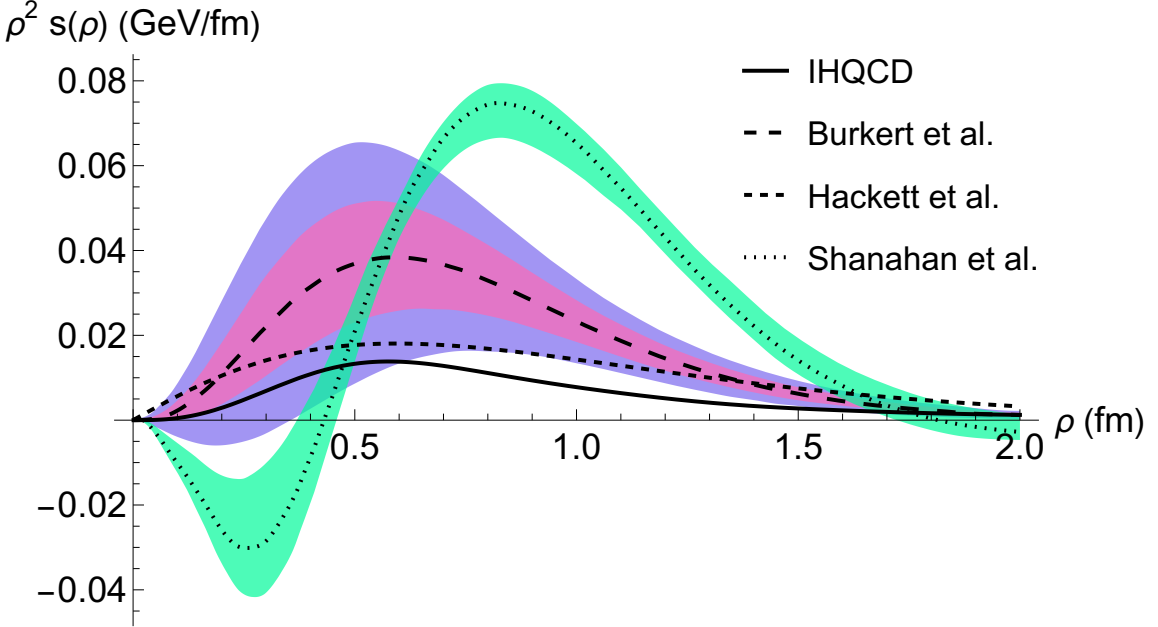


Figure 5. Shear force distributions (4.3) of a proton, as given by different models. Notation as in Fig. 4.

IHQCD and DVCS profiles the angular pressures are more concentrated near the core of the proton, while for the lattice profiles they extend further from the core. Radial pressures are positive in all models, being especially large right outside the core, decreasing towards larger radius. Positivity follows from local stability, see Appendix C. This quantity is proportional to the magnitude of the normal components of forces inside a proton, hence the requirement of positivity is natural. As shown in Fig. 7, the angular pressure changes sign at radii around $\rho \simeq 0.4\text{--}0.5$ fm for all models.

4.2 Proton radius

For a given distribution X , we may define the proton to have a radius $\rho_X = \sqrt{\langle \rho^2 \rangle_X}$. For example, the (expectation value of the square of the) mass-radius of the proton is defined with respect to the energy density, which is given in momentum space as

$$\tilde{\epsilon}(t) \equiv T^{00}(t) = m_N \left[\mathcal{A}(t) - \frac{t}{4m_N^2} (-\mathcal{B}(t) + \mathcal{D}(t)) \right], \quad (4.6)$$

where m_N is the mass of the nucleon. To compute the radius, we Fourier transform back to coordinate-space. With spherical symmetry and $t = -K^2$,

$$\epsilon(\rho) = \frac{m_N}{\pi^2} \int_0^\infty dK \frac{\sin(K\rho)K}{\rho} \left[\mathcal{A}(-K^2) + \frac{K^2}{4m_N^2} (-\mathcal{B}(-K^2) + \mathcal{D}(-K^2)) \right]. \quad (4.7)$$

Then the expectation value of the squared radius is defined as

$$\langle \rho^2 \rangle_{\text{mass}} = \frac{\int d^3\rho \rho^2 \epsilon(\rho)}{\int d^3\rho \epsilon(\rho)}. \quad (4.8)$$

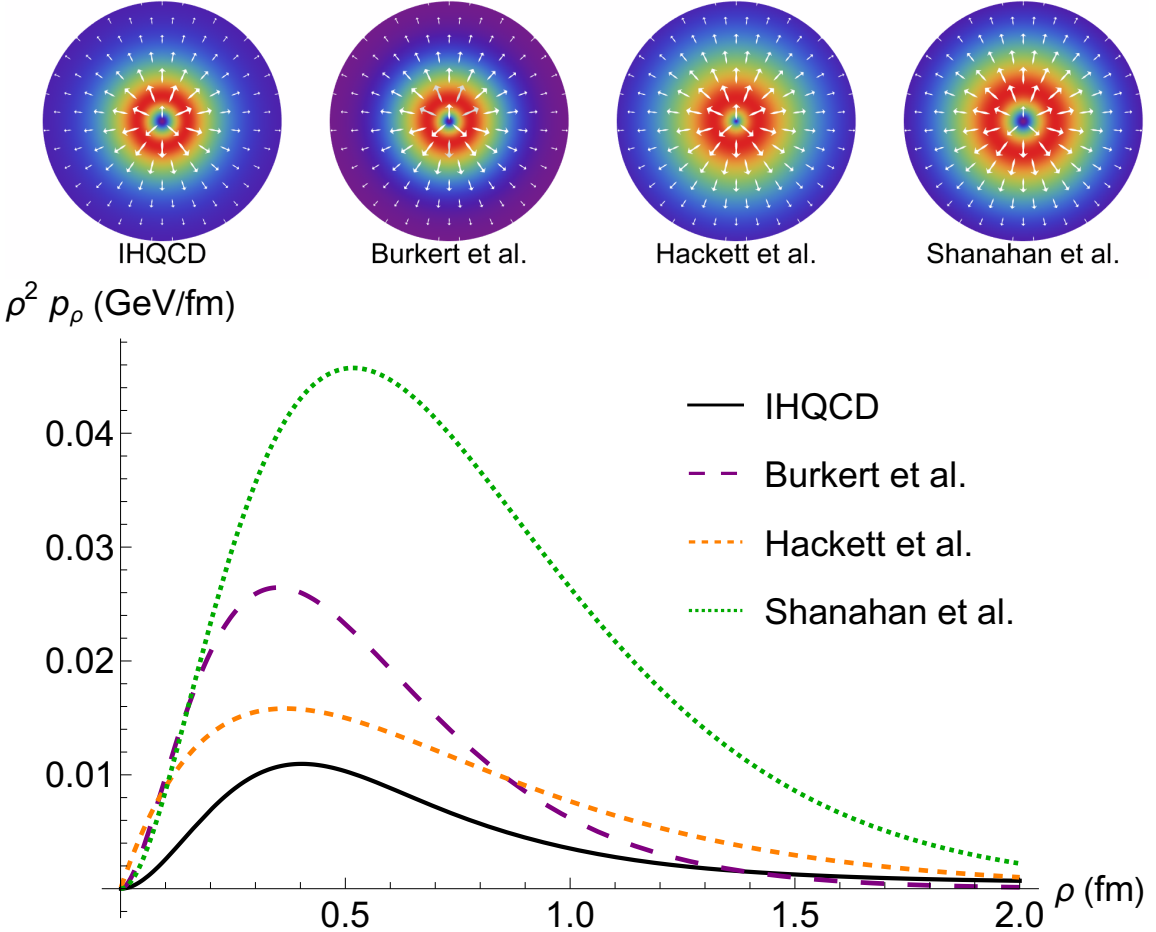


Figure 6. In the upper density plots we show the normalized normal pressures $\rho^2 p_\rho / |\rho^2 p_\rho|_{\max}$ for each model, and in the lower graphs the corresponding absolute normal pressures $\rho^2 p_\rho$ ($\rho \leq 2$ fm) within a proton in different models. We have computed the last three profiles from $\mathcal{D}(t)$'s based on the phenomenological fit of [33], lattice fit of [21], and the lattice fit of [36].

We compute and collect results for this radius $\rho_{\text{mass}} = \sqrt{\langle \rho^2 \rangle_{\text{mass}}}$ for IHQCD and lattice fits, and list them in Table 1.⁶ The value of ρ_{mass} based on [36] was computed by us using the tripole fit from this reference and with the assumption that $\mathcal{B} \approx 0$. The value of [21] was taken directly from the reference.

Another formula for a radius can be derived using the radial pressure p_ρ . Recall that by local stability $p_\rho(\rho) > 0$ for all values of ρ , see Appendix C. With this radial distribution of forces, one may define the mean squared mechanical radius [7],

$$\langle \rho^2 \rangle_{\text{mech}} = \frac{\int d^3\rho \rho^2 p_\rho(\rho)}{\int d^3\rho p_\rho(\rho)} . \quad (4.9)$$

⁶Note that Burkert et al. [32] only fits the form factor $\mathcal{D}(t)$, which is not enough to compute ρ_{mass} .

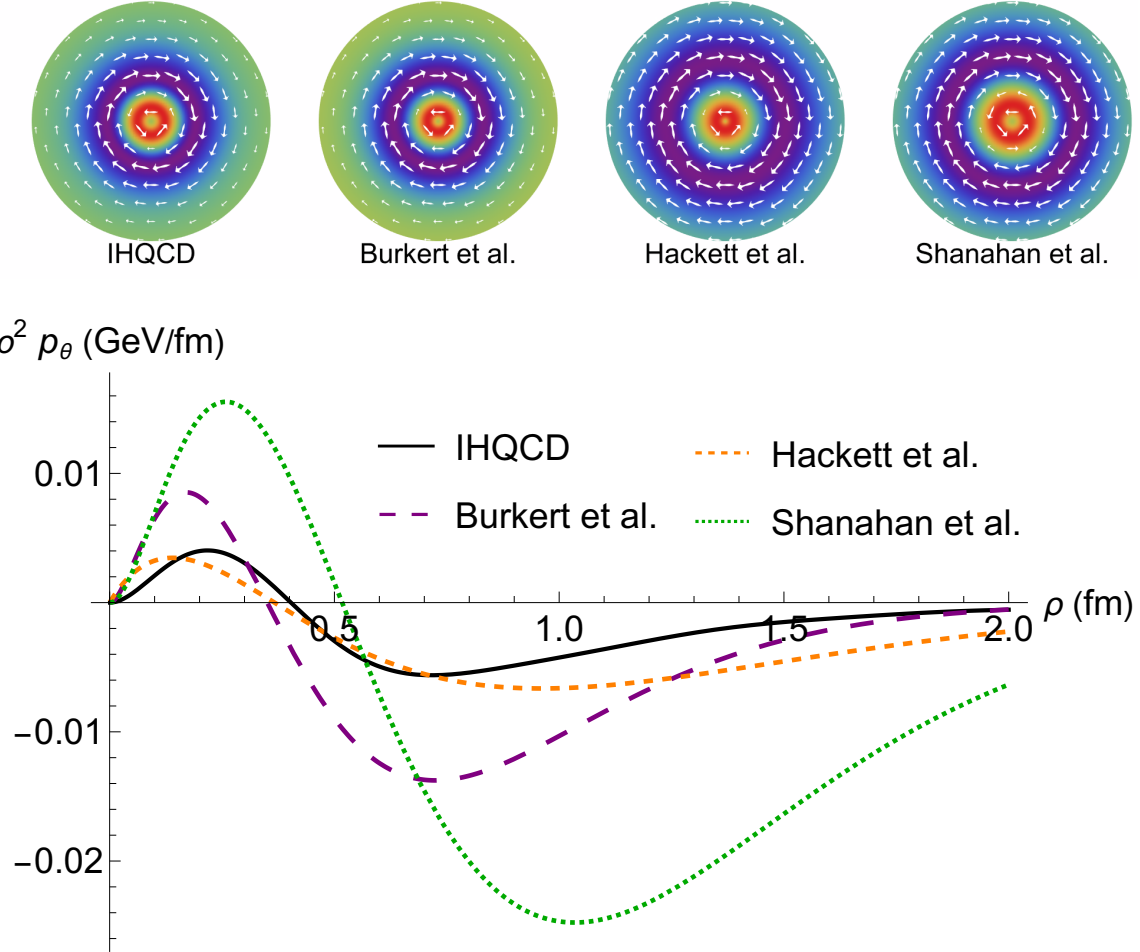


Figure 7. In the upper density plots we show the normalized tangential pressures $\rho^2 p_\theta / |\rho^2 p_\theta|_{\max}$ for each model, and in the lower graphs the corresponding absolute tangential pressures $\rho^2 p_\theta$ ($\rho \leq 2$ fm) within a proton in different models. We have computed the last three profiles from $\mathcal{D}(t)$'s based on the phenomenological fit of [33], lattice fit of [21], and the lattice fit of [36].

We compute and collect results for this radius $\rho_{\text{mech}} = \sqrt{\langle \rho^2 \rangle_{\text{mech}}}$ from IHQCD, lattice and DVCS fits, and list them in Table 1. The value of ρ_{mech} for Burkert et al. [33] was computed by us from the DVCS fit given in the reference. The other values and their error estimates are taken directly from the references.

For a more visual approach, we plot these radii, computed from the fitted profiles of $\mathcal{D}(t)$, in Fig. 8. In the sector of the mechanical and mass radii, the results are shown in the same order as in Table 1. The result for charge radius is the value listed in PDG [44] and the work [45]. The different radii ρ_{mech} , ρ_{mass} , and ρ_{charge} are comparable across models considered in this work. For a recent overview of proton radii in different models, see [46].

Model	ρ_{mech} (fm)	ρ_{mass} (fm)
IHQCD	0.955	0.610
Burkert et al. [33]	0.635	-
Shanahan et al. [36]	0.755 ± 0.007	1.08
Hackett et al. [21]	0.900 ± 0.110	0.820 ± 0.07

Table 1. Proton mechanical and mass radii from different analyses. IHQCD is our result, Burkert et al. is based on a fit to DVCS data, while Shanahan et al. and Hackett et al. are lattice results. See the text for details.

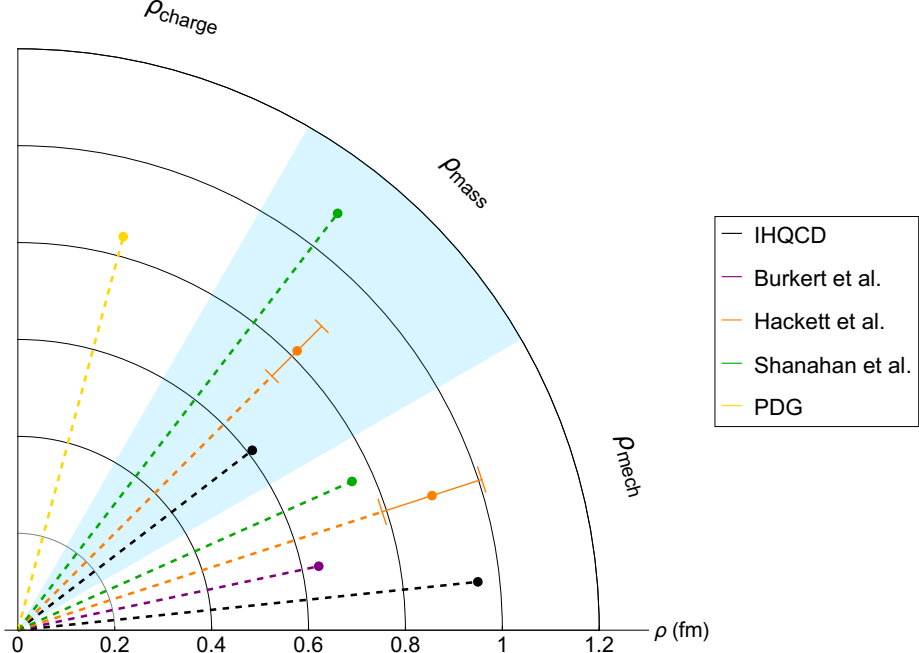


Figure 8. Various determinations of the proton radius. The results are shown in the same order as listed in Table 1. For reference, the value $\rho_{\text{charge}} = 0.841$ fm extracted from muonic hydrogen spectroscopy [45] is also indicated.

5 Conclusions and outlook

We analyzed the structure of the proton using holographic methods, focusing on the gluonic contribution to its gravitational form factors. Since improved holographic QCD is specifically constructed to capture the dynamics of pure Yang–Mills theory, it provided a natural background geometry for this study. In this work, the proton was modeled as a bulk Dirac fermion propagating in a fixed background geometry, which should be viewed as an effective description rather than a fully realistic proton model.

Unlike many earlier holographic analyses, we formulated a consistent gravitational framework in which the relevant form factors were computed directly from the holographic dictionary. The calculation combined scalar and tensor gravitational fluctuations, fermionic bound states, and the diffeomorphism-induced couplings required by general covariance.

The remaining free parameters were fixed by performing a least-squares fit of the form factor $\mathcal{A}(t)$ to lattice data [20, 21], which in turn yielded a nontrivial prediction for $\mathcal{D}(t)$.

Using the extracted form factors, we studied mechanical properties of the proton by exploiting the relation between $\mathcal{D}(t)$ and spatial deformations. This allowed us to define pressure and shear force distributions, which were analyzed and compared with existing lattice and phenomenological studies [10, 20, 21, 32, 33]. We emphasize that such mechanical profiles are not directly measured experimentally, but are inferred under additional assumptions and constraints, and should therefore be interpreted with appropriate care [40, 41]. In the limit $t \rightarrow 0^-$, the structures contributing to $\mathcal{D}(t)$ exhibit a near cancelation; however, since this cancelation is not exact in the present model, an IR pole remains. Despite this behavior, the resulting proton properties are finite and internally consistent. The resulting proton radii estimates in our model were found to be $\rho_{\text{mech}} = 0.95$ fm and $\rho_{\text{mass}} = 0.61$ fm.

Our present holographic setup describes the proton using bulk Dirac fermions propagating in a gravity background dual to pure Yang–Mills theory. While the fermionic fields carry spin, the minimal gravitational couplings included here do not generate the tensor structure required for a nonvanishing Pauli-type GFF, and consequently $\mathcal{B}(t) = 0$ in this model. The vanishing of $\mathcal{B}(t)$ therefore reflects the simplicity of the effective action (2.17) rather than the absence of spin degrees of freedom.

Nevertheless, based on the lattice results of [21], a nonzero $\mathcal{B}(t)$ would contribute a small correction to energy density at low momentum transfer. Incorporating additional couplings that generate a nonvanishing $\mathcal{B}(t)$ would be required for a fully realistic description and is left for future work.

An important direction for future work would be the inclusion of quark degrees of freedom [14, 47]. This would allow access to quark contributions to the gravitational form factors and their associated mechanical properties, as well as to their interplay with the gluonic sector. Lattice results for quark gravitational form factors are already available [21]. Incorporating flavor dependence is essential for addressing spin-dependent structure, but achieving this in a controlled holographic setting remains technically challenging and is the subject of ongoing work [48–53]. In this context, forthcoming measurements at the Electron–Ion Collider are expected to provide valuable constraints on spin-dependent observables [54, 55].

Another future direction would be to develop the model from using the effective five-dimensional fermionic action towards more realistic modeling of the proton. It is known that the proper way of describing baryons in dual gravity model at large N_c is via soliton configurations of gauge fields [56]. Such solitons have indeed been constructed in the extension of the IHQCD model to include flavors, the V-QCD model [25, 57]. Analyzing the form factors by using these solutions would therefore be an important extension of this article.

More broadly, gravitational form factors are closely connected to other nonperturbative observables describing hadron structure, including generalized parton distributions and generalized distribution amplitudes, and indirectly to structure functions. Clarifying these connections within holographic frameworks, and confronting them with lattice and experimental constraints, remains an important open problem for future investigation.

Acknowledgements

We thank Carlos Hoyos and Risto Paatelainen for discussions. N. J. was supported in part by the Research Council of Finland through grant no. 3545331 and the Centre of Excellence in Neutron-Star Physics (project 374062).

A Details on the computation of the form factors

In this appendix we compute and discuss in detail the fluctuation of the fermion action and the resulting vertices. In particular, we find the relevant terms from which to identify the gravitational form factors and discuss how to make the setup parity invariant.

A.1 Varying the fermion action

We start from the fermion action

$$S_F = \mathcal{N} \int d^5x \sqrt{-\det g} e^{-\Phi} \left(\frac{i}{2} \bar{\zeta} e_B^N \gamma^B \partial_N \zeta - \frac{i}{2} (\partial_N \bar{\zeta}) e_B^N \gamma^B \zeta - \mathcal{V}_N(\Phi) \bar{\zeta} \zeta \right), \quad (\text{A.1})$$

which agrees with the proton action in (2.16) and (2.17) but (for reasons that will become clear below) we now denote the fermion field by ζ .

There is a complication regarding the fermion field ζ . Since we do not introduce a background for the fermions it is a probe, and hence interpreted as a fluctuation. So, the action (A.1) is already second order in fluctuations. One might expect that with this setup, it is not necessary to consider transformations of ζ under diffeomorphisms, because the transformation rules are

$$\zeta \mapsto \zeta + \zeta' \xi_r + \partial_\mu \zeta \partial^\mu \xi, \quad \bar{\zeta} \mapsto \bar{\zeta} + \bar{\zeta}' \xi_r + \partial_\mu \bar{\zeta} \partial^\mu \xi, \quad (\text{A.2})$$

where the variation terms are of second order in fluctuations and therefore suppressed with respect to the original fields. However, one needs to be careful, because these rules imply that the second-order terms in fluctuations could change the third-order fluctuation term, which we want to compute. To avoid this change from happening, *i.e.*, in order to remove the mixing of terms of different order under diffeomorphisms, we introduce a fermion field which is invariant up to second order in fluctuations under diffeomorphisms,

$$\Psi = \zeta - \frac{\zeta'}{A'} h - \partial_\mu \zeta \partial^\mu E, \quad \zeta = \Psi + \frac{\Psi'}{A'} h + \partial_\mu \Psi \partial^\mu E. \quad (\text{A.3})$$

Note that this definition is not unique: one could replace the term proportional to h by an analogous term involving h_r , for example. However, this ambiguity does not affect the final result, because the subleading fluctuation terms in (A.3) can be interpreted as a variation of the fermion field, and their effect on the third-order fluctuation term vanishes after one imposes the fermion equation of motion (2.19). This also means that strictly speaking, for our purposes, introducing a gauge invariant fermion field would not be necessary, but we nevertheless find it convenient to do so.

In order to compute the third-order fluctuation term, we write first the second-order term from (A.1) in terms of the covariant field Ψ . After this, we insert the fluctuations

both for the fermions from (A.3) and for the metric from (2.6) in the action and compute the third-order term in fluctuations. The choice of vielbeins e_B^M is not unique. A natural choice is, including only scalar fluctuations up to linear terms,

$$\begin{aligned} e_r^r &= e^{-A} (1 - h_r) , & e_r^\mu &= \frac{1}{2} (\partial^\mu W) e^{-A} , \\ e_\mu^r &= -\frac{1}{2} (\partial_\mu W) e^{-A} , & e_\nu^\mu &= e^{-A} \delta_\nu^\mu (1 - h) + e^{-A} \partial^\mu \partial_\nu E . \end{aligned} \quad (\text{A.4})$$

The expressions for e_r^r and e_ν^μ are the only natural covariant choices here, but the expressions for the other components, e_r^μ and e_μ^r , could also be chosen differently. However, as it turns out, all choices give the same result for the fermion-scalar vertex that we want to compute. A direct yet quite tedious computation gives

$$\begin{aligned} S_F^{(3)} = \mathcal{N} \int d^5x \sqrt{-\det g} e^{-\Phi} \left[& \frac{\Phi'}{A'} \frac{d\mathcal{V}_N(\Phi)}{d\Phi} \bar{\Psi} \Psi \mathcal{F} + \frac{i}{6} \frac{\Phi'^2}{A'^2} e^{-A} (\bar{\Psi}' \gamma^r \Psi - \bar{\Psi} \gamma^r \Psi') \mathcal{F} \right. \\ & \left. + \frac{i}{2} e^{-A} \partial_\mu (\bar{\Psi}' \gamma^\mu \Psi - \bar{\Psi} \gamma^\mu \Psi') \tilde{\mathcal{F}} + \frac{i}{2} e^{-A} (\partial^\mu \bar{\Psi} \gamma^\nu \Psi - \bar{\Psi} \gamma^\mu \partial^\nu \Psi) h_{\mu\nu}^{TT} \right] , \end{aligned} \quad (\text{A.5})$$

where we used Einstein equations both for the background as well as for the fluctuations, and neglected boundary terms.

Einstein equations also imply that $\tilde{\mathcal{F}}$ is the conjugate field of \mathcal{F} , as shown in (2.10). Moreover, they set the third field to zero, $\mathcal{G} = 0$. A second-order action for the dynamical fields, *i.e.*, \mathcal{F} and $h_{\mu\nu}^{TT}$, can be found by expanding the gravity action (see, *e.g.*, [24])

$$S_{\text{IHQCD}}^{(2)} = -M_P^3 N_c^2 \int d^5x \sqrt{-\det g} \left[\frac{\Phi'^2}{A'^2} g^{MN} \partial_M \mathcal{F} \partial_N \mathcal{F} + g^{MN} \partial_M h_{\mu\nu}^{TT} \partial_N h^{TT\mu\nu} \right] . \quad (\text{A.6})$$

Finally, let us check the coupling of the helicity-one fields in gravity to the fermion. We do not expect that these non-propagating fields contribute to the gravitational form factors, but this coupling term provides an additional consistency check of our computations. We follow the conventions of [24], and include the fields A_μ^T and V_μ^T in the fluctuated metric,

$$\begin{aligned} ds^2 = e^{2A(r)} \left[& - \left(\eta_{\mu\nu} + 2h\eta_{\mu\nu} - 2\partial_\mu \partial_\nu E - \partial_{\{\mu} V_{\nu\}}^T - 2h_{\mu\nu}^{TT} \right) dx^\mu dx^\nu \right. \\ & \left. + 2(\partial_\mu W + A_\mu^T) dr dx^\mu + (1 + 2h_r) dr^2 \right] . \end{aligned} \quad (\text{A.7})$$

Here $\partial^\mu V_\mu^T = 0 = \partial^\mu A_\mu^T$. In principle, we also need to add the vectorial contribution in (A.3) to make sure that Ψ remains invariant also in spin-one variations of the coordinates, by writing

$$\zeta = \Psi + \frac{\Psi'}{A'} h + \partial_\mu \Psi \partial^\mu E - \partial^\mu \Psi V_\mu^T . \quad (\text{A.8})$$

However, the contributions from this extra term in the fluctuation of the fermion action again trivially vanish. Therefore, it is enough to consider the variations of the vielbeins in (A.1), extending the expressions (A.4) to include the helicity-one fields. Here, it is important to use the “symmetric” definition of the components e_r^μ and e_μ^r where both of them are nonzero, because otherwise the covariant derivatives of the fermions, which

we have omitted in the action (A.1), would contribute to the vertex. Dropping boundary terms, the coupling between the fermions and the helicity-one fields becomes

$$S_{FVA}^{(3)} = \mathcal{N} \int d^5x \sqrt{-\det g} e^{-\Phi} \frac{i}{4} (-\bar{\Psi} \gamma^\mu \Psi' + \bar{\Psi}' \gamma^\mu \Psi + \bar{\Psi} \gamma^r \partial^\mu \Psi - \partial^\mu \bar{\Psi} \gamma^r \Psi) \left(A_\mu^T - V_\mu^{T'} \right). \quad (\text{A.9})$$

Using the equations of motion for the helicity-one fields from [24], this term vanishes,⁷ as expected.

A.2 Restoring parity

As we pointed out in Section 2.3, restoring parity invariance of the action requires adding two Dirac fermions in the bulk having opposite parities. Doing this explicitly, the total fermion action reads

$$S = \mathcal{N} \int d^5x \sqrt{-\det g} \mathcal{L}_F + \mathcal{N} \int d^4x \sqrt{-\det g^{(4)}} \mathcal{L}_{UV}, \quad (\text{A.10})$$

with

$$\mathcal{L}_F = e^{-\Phi} \left[\frac{i}{2} (\bar{\Psi}_1 e_B^\mu \gamma^B \partial_\mu \Psi_1 + \bar{\Psi}_1 e_B^r \gamma^B \partial_r \Psi_1) + \frac{i}{2} ((\partial_\mu \bar{\Psi}_1) e_B^\mu \gamma^B \Psi_1 + (\partial_r \bar{\Psi}_1) e_B^r \gamma^B \Psi_1) - \mathcal{V}_N(\Phi) \bar{\Psi}_1 \Psi_1 \right] \quad (\text{A.11})$$

$$+ e^{-\Phi} \left[\frac{i}{2} (\bar{\Psi}_2 e_B^\mu \gamma^B \partial_\mu \Psi_2 - \bar{\Psi}_2 e_B^r \gamma^B \partial_r \Psi_2) - \frac{i}{2} ((\partial_\mu \bar{\Psi}_2) e_B^\mu \gamma^B \Psi_2 - (\partial_r \bar{\Psi}_2) e_B^r \gamma^B \Psi_2) - \mathcal{V}_N(\Phi) \bar{\Psi}_2 \Psi_2 \right] \quad (\text{A.12})$$

$$\mathcal{L}_{UV} = e^{-\Phi} (\bar{\Psi}_{1,L} \Psi_{1,R} + \bar{\Psi}_{1,R} \Psi_{1,L}) + e^{-\Phi} (\bar{\Psi}_{2,R} \Psi_{2,L} + \bar{\Psi}_{2,L} \Psi_{2,R}), \quad (\text{A.13})$$

where ψ_1 and ψ_2 are the chiral partner Dirac fields. Note that there are sign changes in the r -derivative terms, effectively obtained by changing the sign of γ^r between the two fields, as we explained in the main text.

Imposing that the fermion fields represent the proton state with momentum p^μ , the expression in (2.22) generalizes to

$$\Psi_1(x, r) = e^{\frac{\Phi(r)}{2} - 2A(r)} [\psi_L(r) u_L(p) + \psi_R(r) u_R(p)] e^{-ip \cdot x} \quad (\text{A.14})$$

$$\Psi_2(x, r) = e^{\frac{\Phi(r)}{2} - 2A(r)} [\psi_R(r) u_L(p) + \psi_L(r) u_R(p)] e^{-ip \cdot x}, \quad (\text{A.15})$$

with the understanding that ψ_L and ψ_R in Ψ_1 are the proton wave functions specified in the main text, so that ψ_L is UV-normalizable. That is, the change of the handedness between Ψ_1 and Ψ_2 amounts to just changing the left- and right-handed solutions,

$$\psi_{R/L} \leftrightarrow \psi_{L/R}. \quad (\text{A.16})$$

⁷The vanishing of the term requires assuming that the gravity fluctuations are massive (*i.e.*, the four-dimensional Fourier modes of the wave functions have a nonzero mass), but as we shall see, this is the case for the wave functions contributing to the form factors.

Following these definitions, let us simplify all terms of $S_F^{(3)}$ in (A.5). The total fluctuation for a two-fermion action reads

$$\begin{aligned}
S_F^{(3)} = \mathcal{N} \int d^5x \sqrt{-\det g} e^{-\Phi} & \left[\frac{\Phi'}{A'} \frac{d\mathcal{V}_N(\Phi)}{d\Phi} (\bar{\Psi}_1 \Psi_1 + \bar{\Psi}_2 \Psi_2) \mathcal{F} \right. \\
& + \frac{i}{6} \frac{\Phi'^2}{A'^2} e^{-A} (\bar{\Psi}'_1 \gamma^r \Psi_1 - \bar{\Psi}_1 \gamma^r \Psi'_1 - \bar{\Psi}'_2 \gamma^r \Psi_2 + \bar{\Psi}_2 \gamma^r \Psi'_2) \mathcal{F} \\
& + \frac{i}{2} e^{-A} \partial_\mu (\bar{\Psi}'_1 \gamma^\mu \Psi_1 - \bar{\Psi}_1 \gamma^\mu \Psi'_1 + \bar{\Psi}'_2 \gamma^\mu \Psi_2 - \bar{\Psi}_2 \gamma^\mu \Psi'_2) \tilde{\mathcal{F}} \\
& \left. + \frac{i}{2} e^{-A} (\partial^\mu \bar{\Psi}_1 \gamma^\nu \Psi_1 - \bar{\Psi}_1 \gamma^\mu \partial^\nu \Psi_1 + \partial^\mu \bar{\Psi}_2 \gamma^\nu \Psi_2 - \bar{\Psi}_2 \gamma^\mu \partial^\nu \Psi_2) h_{\mu\nu}^{TT} \right] . \tag{A.17}
\end{aligned}$$

First, consider the terms on the last line as an explicit example. The terms involving Ψ_1 are

$$\begin{aligned}
& i(\partial^\mu \bar{\Psi}_1 \gamma^\nu \Psi_1 - \bar{\Psi}_1 \gamma^\mu \partial^\nu \Psi_1) \\
& = p_2^\mu (\psi_L \bar{u}_L(p_2) + \psi_R \bar{u}_R(p_2)) \gamma^\nu (\psi_L u_L(p_1) + \psi_R u_R(p_1)) e^{i(p_2-p_1)\cdot x} e^{\Phi-4A} \\
& \quad + (\psi_L \bar{u}_L(p_2) + \psi_R \bar{u}_R(p_2)) \gamma^\mu p_1^\nu (\psi_L u_L(p_1) + \psi_R u_R(p_1)) e^{i(p_2-p_1)\cdot x} e^{\Phi-4A} \\
& = p_2^\mu \left[\psi_L^2 \bar{u}_L(p_2) \gamma^\nu u_L(p_1) + \psi_R^2 \bar{u}_L(p_2) \frac{p_2^\mu}{m_N} \gamma^\nu \frac{p_1^\mu}{m_N} u_L(p_1) \right] e^{ik\cdot x} e^{\Phi-4A} \\
& \quad + p_1^\nu \left[\psi_L^2 \bar{u}_L(p_2) \gamma^\mu u_L(p_1) + \psi_R^2 \bar{u}_L(p_2) \frac{p_2^\mu}{m_N} \gamma^\mu \frac{p_1^\mu}{m_N} u_L(p_1) \right] e^{ik\cdot x} e^{\Phi-4A} , \tag{A.18}
\end{aligned}$$

where p_1 (p_2) is the momentum of the incoming (outgoing) proton and recall that $k = p_2 - p_1$ is the exchanged momentum.

Now, the result for Ψ_2 follows by changing the handedness of both bound modes. Doing this explicitly gives

$$\begin{aligned}
& i(\partial^\mu \bar{\Psi}_2 \gamma^\nu \Psi_2 - \bar{\Psi}_2 \gamma^\mu \partial^\nu \Psi_2) \\
& = p_2^\mu \left[\psi_R^2 \bar{u}_R(p_2) \frac{p_2^\mu}{m_N} \gamma^\nu \frac{p_1^\mu}{m_N} u_R(p_1) + \psi_L^2 \bar{u}_R(p_2) \gamma^\nu u_R(p_1) \right] e^{ik\cdot x} e^{\Phi-4A} \\
& \quad + p_1^\nu \left[\psi_R^2 \bar{u}_R(p_2) \frac{p_2^\mu}{m_N} \gamma^\mu \frac{p_1^\mu}{m_N} u_R(p_1) + \psi_L^2 \bar{u}_R(p_2) \gamma^\mu u_R(p_1) \right] e^{ik\cdot x} e^{\Phi-4A} . \tag{A.19}
\end{aligned}$$

These contributions (A.18) and (A.19) may be immediately combined by using $u_R(p) + u_L(p) = u(p)$. We obtain

$$\begin{aligned}
& i(\partial^\mu \bar{\Psi}_1 \gamma^\nu \Psi_1 - \bar{\Psi}_1 \gamma^\mu \partial^\nu \Psi_1 + \partial^\mu \bar{\Psi}_2 \gamma^\nu \Psi_2 - \bar{\Psi}_2 \gamma^\mu \partial^\nu \Psi_2) \\
& = (\psi_R^2 + \psi_L^2) \bar{u}(p_2) (p_2^\mu \gamma^\nu + p_1^\nu \gamma^\mu) u(p_1) e^{ik\cdot x} e^{\Phi-4A} , \tag{A.20}
\end{aligned}$$

where we also used $\not{p} u(p) = m_N u(p)$. In addition, we may write

$$p^\mu \gamma^\nu = \frac{p^{\{\mu} \gamma^{\nu\}}}{2} - \frac{1}{4} \eta^{\mu\nu} p_\alpha \gamma^\alpha . \tag{A.21}$$

We contract (A.20) with $h_{\mu\nu}^{TT}$, and by transverse-tracelessness, the second part of (A.21) does not contribute. Hence we find

$$\begin{aligned}
& (\psi_R^2 + \psi_L^2) \bar{u}(p_2) (p_2^\mu \gamma^\nu + p_1^\nu \gamma^\mu) u(p_1) e^{i(p_2-p_1)\cdot x} e^{\Phi-4A} h_{\mu\nu}^{TT} \\
& = 2(\psi_R^2 + \psi_L^2) \bar{u}(p_2) \frac{P^{\{\mu} \gamma^{\nu\}}}{2} u(p_1) e^{ik\cdot x} e^{\Phi-4A} h_{\mu\nu}^{TT} . \tag{A.22}
\end{aligned}$$

We simplify the rest of the terms in $S_F^{(3)}$ in a similar manner. The resulting expressions are

$$\begin{aligned} \bar{\Psi}_1 \Psi_1 + \bar{\Psi}_2 \Psi_2 &= 2\bar{u}(p_2)\psi_R \psi_L u(p_1) e^{ik \cdot x} e^{\Phi - 4A} \\ \bar{\Psi}'_1 \gamma^r \Psi_1 - \bar{\Psi}_1 \gamma^r \Psi'_1 - \bar{\Psi}'_2 \gamma^r \Psi_2 + \bar{\Psi}_2 \gamma^r \Psi'_2 &= 2\bar{u}(p_2)(\psi'_L \psi_R - \psi_L \psi'_R) u(p_1) e^{ik \cdot x} e^{\Phi - 4A} \\ \bar{\Psi}'_1 \gamma^\mu \Psi_1 - \bar{\Psi}_1 \gamma^\mu \Psi'_1 + \bar{\Psi}'_2 \gamma^\mu \Psi_2 - \bar{\Psi}_2 \gamma^\mu \Psi'_2 &= 0 . \end{aligned} \quad (\text{A.23})$$

Substituting the results (A.22) and (A.23) into $S_F^{(3)}$ yields

$$\begin{aligned} S_F^{(3)} &= \mathcal{N} \int d^5x \left[2 \frac{\Phi'}{A'} e^A \frac{d\mathcal{V}_N(\Phi)}{d\Phi} \bar{u}(p_2) \psi_L \psi_R u(p_1) \mathcal{F} + \frac{2}{6} \left(\frac{\Phi'}{A'} \right)^2 \bar{u}(p_2) (\psi'_L \psi_R - \psi_L \psi'_R) u(p_1) \mathcal{F} \right. \\ &\quad \left. + (\psi_R^2 + \psi_L^2) \bar{u}(p_2) \frac{P^{\{\mu\gamma^\nu\}}}{2} u(p_1) h_{\mu\nu}^{TT} \right] e^{ik \cdot x} . \end{aligned} \quad (\text{A.24})$$

Further, inserting here (3.11) and (3.12) we find

$$\begin{aligned} S_{F \text{ o-s}}^{(3)} &= \mathcal{N} \int d^5x e^{ik \cdot x} \int \frac{d^4p}{(2\pi)^4} e^{-ip \cdot x} \\ &\quad \times \left[2 \frac{\Phi'}{A'} e^A \frac{d\mathcal{V}_N(\Phi)}{d\Phi} \bar{u}(p_2) \psi_L \psi_R u(p_1) \hat{f}_s(p, r) \frac{1}{6} (\eta^{\mu\nu} - p^\mu p^\nu / p^2) \int d^4y e^{ip \cdot y} \delta\eta_{\mu\nu}(y) \right. \\ &\quad + \frac{2}{6} \left(\frac{\Phi'}{A'} \right)^2 \bar{u}(p_2) (\psi'_L \psi_R - \psi_L \psi'_R) u(p_1) \hat{f}_s(p, r) \frac{1}{6} (\eta^{\mu\nu} - p^\mu p^\nu / p^2) \int d^4y e^{ip \cdot y} \delta\eta_{\mu\nu}(y) \\ &\quad \left. + (\psi_R^2 + \psi_L^2) \bar{u}(p_2) \frac{P^{\{\mu\gamma^\nu\}}}{2} u(p_1) \hat{h}_s^{TT}(p, r) \left(-\frac{1}{2} \hat{\epsilon}_{\mu\nu}^{TT, \alpha\beta}(p) \right) \int d^4y e^{ip \cdot y} \delta\eta_{\alpha\beta}(y) \right] . \end{aligned} \quad (\text{A.25})$$

B Asymptotic solutions

B.1 IR asymptotics of the background

In the IR (large coupling λ), a generic expansion of the potential, which covers physically motivated choices, is [18, 19]

$$V(\lambda) \approx v_0 \lambda^{2Q} \log^P(\lambda) \left(1 + \sum_{i=1}^{\infty} \frac{v_i}{(\log \lambda)^i} \right) . \quad (\text{B.1})$$

We adopt a convention where the UV expansion coefficients are denoted by V_i (see below) and IR expansion coefficients are denoted by v_i , $i = 0, 1, 2, \dots$. The IR expansions for $A(r)$ and $\Phi(r)$ within V-QCD can be found from [47]:

$$A = -\left(\frac{r-r_0}{R}\right)^\alpha + A_0 - \frac{1}{2}\frac{P}{1-P}\log\left(\frac{R}{r-r_0}\right) + \frac{5}{6} + \frac{P}{4} + \frac{1}{2}P\log\frac{3}{2} + \frac{2V_1}{3PV_0} + \frac{-52P^2V_0^2 + 4P^3V_0^2 + 27P^4V_0^2 + 64V_1^2 - 64PV_1^2 + 128PV_0V_2}{288P(1+P)V_0^2}\left(\frac{R}{r-r_0}\right)^\alpha + \dots \quad (B.2)$$

$$\log \lambda = \frac{3}{2}\left(\frac{r-r_0}{R}\right)^\alpha - \frac{5}{4} - \frac{3P}{8} - \frac{V_1}{PV_0} + \frac{-20P^2V_0^2 - 40P^3V_0^2 + 9P^4V_0^2 - 64V_1^2 + 64PV_1^2 - 128PV_0V_2}{192P(1+P)V_0^2}\left(\frac{R}{r-r_0}\right)^\alpha + \dots, \quad (B.3)$$

where the parameters α and A_0 are defined as

$$\alpha = \frac{1}{1-P}, \quad e^{A_0} = \frac{2^P 3^{1-P}}{(1-P)\sqrt{V_0}R}, \quad (B.4)$$

and R is an arbitrary scale we set to unity, $R = 1$. In our case, we have $Q = 2/3$, $P = 1/2$. Thus,

$$\begin{aligned} A(r) &= -\frac{r^2}{R^2} + \frac{1}{2}\log\frac{r}{R} - \log R - \frac{1}{2}\log v_0 + \frac{5}{4}\log 2 + \frac{3}{4}\log 3 \\ &\quad + \frac{23}{24} + \frac{4v_1}{3} + \frac{R^2(-173 + 512v_1^2 + 1024v_2)}{3456r^2} + \mathcal{O}\left(\frac{1}{r^4}\right) \\ \Phi(r) &= \frac{3}{2}\frac{r^2}{R^2} - \frac{23}{16} - 2v_1 - \frac{R^2(151 + 512v_1^2 + 1024v_2)}{2304r^2} + \mathcal{O}\left(\frac{1}{r^4}\right). \end{aligned} \quad (B.5)$$

The updated gravity potential we used was given above in (2.2), and has been adopted from [25]. Contributions to the IR expansion stem from the last term in the potential (2.2). The connection of the expansion coefficient v_0 to the parameters in this formula is $v_0 = \frac{3V_{\text{IR}}}{4\pi^{8/3}}$. Inserting the numerical values of the parameters, the expansion coefficients up to fourth order become

$$v_0 \approx 0.2562, \quad v_1 \approx -1.664, \quad v_2 \approx -1.384, \quad v_3 \approx -2.303, \quad v_4 \approx -4.790. \quad (B.6)$$

Inserting these numerical values in (B.5) gives the asymptotics

$$\begin{aligned} A(r) &\approx -r^2 - 1.11123 + \frac{1}{4}\log(r^2) - \frac{0.0500579}{r^2} + \mathcal{O}\left(\frac{1}{r^4}\right) \\ \Phi(r) &\approx \frac{3}{2}r^2 + 1.89014 - \frac{0.0655382}{r^2} + \mathcal{O}\left(\frac{1}{r^4}\right). \end{aligned} \quad (B.7)$$

B.2 Near-boundary asymptotics of the background

In the UV (weak coupling λ), we expand the potential as

$$V(\lambda) \approx \frac{12}{\ell^2} \left(1 + \sum_{i=1}^{\infty} V_i \lambda^i\right). \quad (B.8)$$

The background UV expansions are found from [58] and read

$$\begin{aligned}
A(r) &= -\log\left(\frac{r}{\ell}\right) + \frac{4}{9\log(r\Lambda)} \\
&\quad + \frac{\frac{1}{162}\left(95 - \frac{64V_2}{V_1^2}\right) + \frac{1}{81}\log(-\log(r\Lambda))\left(-23 + \frac{64V_2}{V_1^2}\right)}{\log^2(r\Lambda)} + \mathcal{O}\left(\frac{1}{\log^3(r\Lambda)}\right) \\
\exp[\Phi(r)] &= \frac{8}{9\log(r\Lambda)V_1} + \frac{\log(-\log(r\Lambda))\left(\frac{46}{81} - \frac{128V_2}{81V_1^2}\right)}{\log^2(r\Lambda)V_1} + \mathcal{O}\left(\frac{1}{\log^3(r\Lambda)}\right).
\end{aligned} \tag{B.9}$$

For the potential used in this article, the numerical values of the first four coefficients are explicitly

$$V_1 = 0.4953, \quad V_2 = 1.220 \times 10^{-2}, \quad V_3 = -4.376 \times 10^{-4}, \quad V_4 = 1.570 \times 10^{-5}. \tag{B.10}$$

Inserting these values and setting $\ell = 1$ the expansions become

$$\begin{aligned}
A(r) &\approx -\log r + \frac{4}{9\log(r\Lambda)} + \frac{0.35078 + 0.18733\log(-\log(r\Lambda))}{\log^2(r\Lambda)} \\
\exp[\Phi(r)] &\approx -\frac{21.534}{\log(r\Lambda)} - \frac{9.0762\log(-\log(r\Lambda))}{\log^2(r\Lambda)}.
\end{aligned} \tag{B.11}$$

B.3 Near-boundary asymptotics of the fermion wave functions

In order to analyze UV-normalizability of the fermion action (2.17), we search for asymptotic solutions to the Eq. (2.25) at weak coupling.

We first expand the left- and right-handed potentials in (2.29) near UV, $r \rightarrow 0$. We use the UV expansions of $\Phi(r)$ and $A(r)$ presented in (B.11). Expanding in r , $-\log r$, and $\log(-\log r)$ yields asymptotic formulas

$$\mathcal{V}_L \sim \beta \frac{\log(-\log(r))^{1/4}}{r^2(-\log(r))^{2/3}}, \quad \mathcal{V}_R \sim -\beta \frac{\log(-\log(r))^{1/4}}{r^2(-\log(r))^{2/3}}, \tag{B.12}$$

where β is a constant. Hence, the differential equations (2.25) in the asymptotic limit $r \rightarrow 0$ read

$$\psi''_{L,R}(r) \pm \beta \frac{\log(-\log(r))^{1/4}}{r^2(-\log(r))^{2/3}} \psi_{L,R}(r) \approx 0, \tag{B.13}$$

as the mass term is subleading, and plus and minus are for the left- and right-handed modes, respectively.

We first search for the asymptotics of the VEV part of the solution by inserting an *Ansatz* $\psi = r \cdot e^{f(\log(-\log(r)))}$ and solving the resulting leading differential equation for the arbitrary function f . This gives the asymptotics for the UV-normalizable left- and right-handed modes as

$$\psi_{L,R}(r) \sim r \cdot \exp\left(\mp 3\beta\left((- \log(r))^{1/3} \log(-\log(r))^{1/4}\right)\right). \tag{B.14}$$

Likewise, we search for the asymptotics of the source part of the solution by setting the *Ansatz* to $\psi = e^{f(\log(-\log(r)))}$. Solving again for the leading behavior gives the non-normalizable solutions

$$\psi_{L,R}(r) \sim \exp\left(\pm 3\beta\left((- \log(r))^{1/3} \log(- \log(r))^{1/4}\right)\right). \quad (\text{B.15})$$

In general, the leading order asymptotics therefore read

$$\begin{aligned} \psi_L &\sim A_L e^{3\beta(-\log r)^{1/3} \log(-\log r)^{1/4}} + B_L r e^{-3\beta(-\log r)^{1/3} \log(-\log r)^{1/4}} \\ \psi_R &\sim A_R e^{-3\beta(-\log r)^{1/3} \log(-\log r)^{1/4}} + B_R r e^{3\beta(-\log r)^{1/3} \log(-\log r)^{1/4}}, \end{aligned} \quad (\text{B.16})$$

where $A_{L/R}$ and $B_{L/R}$ are *a priori* free constants for the source and VEV asymptotic solutions, respectively. However, given the relations in Eq. (2.24), there are only two independent parameters. Relations between constants in (B.16) can be explicitly solved by inserting the asymptotic solutions in these equations. We find

$$A_R = B_L/m_n, \quad B_R = -A_L \cdot m_n, \quad (\text{B.17})$$

where $m_n = \sqrt{p^2}$ is the mass of the nucleon state. Inserting these relations into the asymptotic formulas, the final expressions read

$$\begin{aligned} \psi_L &\sim A_L \cdot \exp\left(3\beta\left((- \log(r))^{1/3} \log(- \log(r))^{1/4}\right)\right) \\ &\quad + B_L r \cdot \exp\left(-3\beta\left((- \log(r))^{1/3} \log(- \log(r))^{1/4}\right)\right) \\ \psi_R &\sim \frac{B_L}{m_n} \cdot \exp\left(-3\beta\left((- \log(r))^{1/3} \log(- \log(r))^{1/4}\right)\right) \\ &\quad - A_L m_n r \cdot \exp\left(3\beta\left((- \log(r))^{1/3} \log(- \log(r))^{1/4}\right)\right). \end{aligned} \quad (\text{B.18})$$

C Mechanical consistency

There exists a wide variety of mechanical consistency checks, many of which result from a single master integral [7]. This integral comes from a generic condition on the conservation of the energy-momentum tensor, namely

$$\int_V d^3\rho (\nabla^i T^{ij}) X^{jklm\dots} = 0, \quad (\text{C.1})$$

where X is some smooth tensor. Inserting here $X^j = \rho^j f(\rho)$, where $f(\rho)$ is an analytic function, the resulting master integral reads

$$I[f(\rho)] \equiv \int_0^\infty d\rho \rho^2 \left(\frac{2}{3} \rho s(\rho) \frac{df(\rho)}{d\rho} + \rho p(\rho) \frac{df(\rho)}{d\rho} + 3p(\rho) f(\rho) \right) = 0, \quad (\text{C.2})$$

where $p(\rho)$ and $s(\rho)$ are given in (4.3). Now, inserting different profiles for $f(\rho)$ results in different consistency conditions. For example, choosing $f(\rho) = 1$, one obtains the *von Laue stability condition*,

$$\int_0^\infty d\rho \rho^2 p(\rho) = 0. \quad (\text{C.3})$$

Physically this states that the nucleon must be stable, neither collapsing nor expanding.

Using different integer exponents $f(\rho) = \rho^N$ in (C.2), we obtain Mellin-moment relations of the form

$$\int_0^\infty d\rho \left[\frac{2}{3}Ns(\rho) + (N+3)p(\rho) \right] \rho^{N+2} = 0 . \quad (\text{C.4})$$

If $\mathcal{D}(t)$ does not vanish quickly enough at high t , the integrals in the stability conditions may be divergent. The behavior predicted by QCD counting rules, $\mathcal{D}(t) \sim 1/t^3$ at high momentum exchange, is sufficient for the convergence of the stability conditions down to $N = -2$.

Nothing prevents one to also input more exotic functions into the master integral, such as the pressure profile itself. This results in a nonlinear consistency condition

$$\int_0^\infty d\rho \rho^2 \left(\frac{2}{3}s^2(\rho) - \frac{3}{2}p^2(\rho) \right) = 0 , \quad (\text{C.5})$$

which also must be fulfilled by all consistent pressure and shear profiles.

References

- [1] A. Accardi et al., *Electron Ion Collider: The Next QCD Frontier: Understanding the glue that binds us all*, *Eur. Phys. J. A* **52** (2016) 268 [[1212.1701](#)].
- [2] X. Ji, F. Yuan and Y. Zhao, *What we know and what we don't know about the proton spin after 30 years*, *Nature Rev. Phys.* **3** (2021) 27 [[2009.01291](#)].
- [3] H1, ZEUS collaboration, *Combined measurement and QCD analysis of the inclusive $e^- p$ scattering cross sections at HERA*, *PoS DIS2010* (2010) 035.
- [4] J. Collins, *Foundations of perturbative QCD*, Cambridge monographs on particle physics, nuclear physics, and cosmology, Cambridge Univ. Press, New York, NY (2011), [10.1017/CBO9780511975592](#).
- [5] K. Goeke, M.V. Polyakov and M. Vanderhaeghen, *Hard exclusive reactions and the structure of hadrons*, *Prog. Part. Nucl. Phys.* **47** (2001) 401 [[hep-ph/0106012](#)].
- [6] A.V. Ramallo, *Introduction to the AdS/CFT correspondence*, *Springer Proc. Phys.* **161** (2015) 411 [[1310.4319](#)].
- [7] M.V. Polyakov and P. Schweitzer, *Forces inside hadrons: pressure, surface tension, mechanical radius, and all that*, *Int. J. Mod. Phys. A* **33** (2018) 1830025 [[1805.06596](#)].
- [8] Z. Abidin and C.E. Carlson, *Nucleon electromagnetic and gravitational form factors from holography*, *Phys. Rev. D* **79** (2009) 115003 [[0903.4818](#)].
- [9] Z. Abidin and C.E. Carlson, *Gravitational form factors of vector mesons in an AdS/QCD model*, *Phys. Rev. D* **77** (2008) 095007 [[0801.3839](#)].
- [10] K.A. Mamo and I. Zahed, *Diffractive photoproduction of J/ψ and Υ using holographic QCD: gravitational form factors and GPD of gluons in the proton*, *Phys. Rev. D* **101** (2020) 086003 [[1910.04707](#)].
- [11] M. Fujita, Y. Hatta, S. Sugimoto and T. Ueda, *Nucleon D-term in holographic quantum chromodynamics*, *PTEP* **2022** (2022) 093B06 [[2206.06578](#)].

- [12] Y. Li and J.P. Vary, *Stress inside the pion in holographic light-front QCD*, *Phys. Rev. D* **109** (2024) L051501 [[2312.02543](#)].
- [13] S. Sugimoto and T. Tsukamoto, *Energy-Momentum Tensor and D-term of Baryons in Top-down Holographic QCD*, [2503.19492](#).
- [14] J. Deng and D. Hou, *Nucleon structure from an AdS/QCD model in the Veneziano limit*, *Phys. Rev. D* **112** (2025) 036011 [[2502.00771](#)].
- [15] Z. Liu and A. Watanabe, *Gravitational form factor of the kaon in holographic QCD*, *Phys. Rev. D* **112** (2025) 114032 [[2503.18747](#)].
- [16] K. Hashimoto, T. Sakai and S. Sugimoto, *Holographic Baryons: Static Properties and Form Factors from Gauge/String Duality*, *Prog. Theor. Phys.* **120** (2008) 1093 [[0806.3122](#)].
- [17] U. Gürsoy, E. Kiritsis, L. Mazzanti, G. Michalogiorgakis and F. Nitti, *Improved Holographic QCD*, *Lect. Notes Phys.* **828** (2011) 79 [[1006.5461](#)].
- [18] U. Gürsoy and E. Kiritsis, *Exploring improved holographic theories for QCD: Part I*, *JHEP* **02** (2008) 032 [[0707.1324](#)].
- [19] U. Gürsoy, E. Kiritsis and F. Nitti, *Exploring improved holographic theories for QCD: Part II*, *JHEP* **02** (2008) 019 [[0707.1349](#)].
- [20] P.E. Shanahan and W. Detmold, *Gluon gravitational form factors of the nucleon and the pion from lattice QCD*, *Phys. Rev. D* **99** (2019) 014511 [[1810.04626](#)].
- [21] D.C. Hackett, D.A. Pefkou and P.E. Shanahan, *Gravitational Form Factors of the Proton from Lattice QCD*, *Phys. Rev. Lett.* **132** (2024) 251904 [[2310.08484](#)].
- [22] A. Amorim, M.S. Costa and M. Järvinen, *Regge theory in a holographic dual of QCD in the Veneziano limit*, *JHEP* **07** (2021) 065 [[2102.11296](#)].
- [23] A.W. Peet and J. Polchinski, *UV / IR relations in AdS dynamics*, *Phys. Rev. D* **59** (1999) 065011 [[hep-th/9809022](#)].
- [24] E. Kiritsis and F. Nitti, *On massless 4D gravitons from asymptotically AdS(5) space-times*, *Nucl. Phys. B* **772** (2007) 67 [[hep-th/0611344](#)].
- [25] M. Järvinen, E. Kiritsis, F. Nitti and E. Préau, *The V-QCD baryon: numerical solution and baryon spectrum*, *JHEP* **05** (2023) 081 [[2212.06747](#)].
- [26] V.F. Foit, D. Kabat and G. Lifschytz, *Bulk reconstruction for spinor fields in AdS/CFT*, *JHEP* **02** (2020) 129 [[1912.00952](#)].
- [27] R. Contino and A. Pomarol, *Holography for fermions*, *JHEP* **11** (2004) 058 [[hep-th/0406257](#)].
- [28] N.W.M. Plantz, F. García Flórez and H.T.C. Stoof, *Massive Dirac fermions from holography*, *JHEP* **04** (2018) 123 [[1802.04191](#)].
- [29] M. Henningsson and K. Sfetsos, *Spinors and the AdS / CFT correspondence*, *Phys. Lett. B* **431** (1998) 63 [[hep-th/9803251](#)].
- [30] C. Hoyos, N. Jokela and D. Logares, *Scattering length from holographic duality*, *Phys. Rev. D* **101** (2020) 046028 [[1910.13929](#)].
- [31] S.S. Gubser, I.R. Klebanov and A.M. Polyakov, *Gauge theory correlators from noncritical string theory*, *Phys. Lett. B* **428** (1998) 105 [[hep-th/9802109](#)].

[32] V.D. Burkert, L. Elouadrhiri and F.X. Girod, *The pressure distribution inside the proton*, *Nature* **557** (2018) 396.

[33] V.D. Burkert, L. Elouadrhiri and F.X. Girod, *Determination of shear forces inside the proton*, [2104.02031](#).

[34] CLAS collaboration, *Measurement of Deeply virtual Compton scattering beam-spin asymmetries*, *Phys. Rev. Lett.* **100** (2008) 162002 [[0711.4805](#)].

[35] CLAS collaboration, *Cross sections for the exclusive photon electroproduction on the proton and Generalized Parton Distributions*, *Phys. Rev. Lett.* **115** (2015) 212003 [[1504.02009](#)].

[36] P.E. Shanahan and W. Detmold, *Pressure Distribution and Shear Forces inside the Proton*, *Phys. Rev. Lett.* **122** (2019) 072003 [[1810.07589](#)].

[37] R. Stegeman and R. Zwicky, *Gravitational D-Form Factor: The σ -Meson as a Dilaton confronted with Lattice Data*, [2508.18537](#).

[38] R. Stegeman and R. Zwicky, *Gluon Gravitational D-Form Factor: The σ -Meson as a Dilaton Confronted with Lattice Data II*, [2512.12315](#).

[39] A. Mejia and P. Schweitzer, *Energy-momentum tensor form factor $D(t)$ of proton and neutron*, [2511.21916](#).

[40] K. Kumerički and D. Mueller, *Deeply virtual Compton scattering at small x_B and the access to the GPD H* , *Nucl. Phys. B* **841** (2010) 1 [[0904.0458](#)].

[41] K. Kumerički, *Measurability of pressure inside the proton*, *Nature* **570** (2019) E1.

[42] K. Tanaka, *Operator relations for gravitational form factors of a spin-0 hadron*, *Phys. Rev. D* **98** (2018) 034009 [[1806.10591](#)].

[43] S.J. Brodsky and G.R. Farrar, *Scaling Laws at Large Transverse Momentum*, *Phys. Rev. Lett.* **31** (1973) 1153.

[44] PARTICLE DATA GROUP collaboration, *Review of particle physics*, *Phys. Rev. D* **110** (2024) 030001.

[45] A. Antognini et al., *Proton Structure from the Measurement of $2S - 2P$ Transition Frequencies of Muonic Hydrogen*, *Science* **339** (2013) 417.

[46] MMGPDs collaboration, *Can we determine the exact size of the nucleon?: A comprehensive study of different radii*, *Nucl. Phys. B* **1017** (2025) 116962 [[2503.08847](#)].

[47] M. Järvinen and E. Kiritsis, *Holographic Models for QCD in the Veneziano Limit*, *JHEP* **03** (2012) 002 [[1112.1261](#)].

[48] R. Alvares, C. Hoyos and A. Karch, *An improved model of vector mesons in holographic QCD*, *Phys. Rev. D* **84** (2011) 095020 [[1108.1191](#)].

[49] Z. Fang, Y.-L. Wu and L. Zhang, *Chiral Phase Transition with 2+1 quark flavors in an improved soft-wall AdS/QCD Model*, *Phys. Rev. D* **98** (2018) 114003 [[1805.05019](#)].

[50] R.-G. Cai, S. He, L. Li and Y.-X. Wang, *Probing QCD critical point and induced gravitational wave by black hole physics*, *Phys. Rev. D* **106** (2022) L121902 [[2201.02004](#)].

[51] L. Zhang and M. Huang, *Holographic cold dense matter constrained by neutron stars*, *Phys. Rev. D* **106** (2022) 096028 [[2209.00766](#)].

[52] M. Järvinen and T. Mitra, *Quark flavors in hot and dense holographic QCD: setup and comparison to data*, [2507.08087](#).

- [53] J.-Y. Shen, X.-Y. Liu, J.-R. Wu, Y.-L. Wu and Z. Fang, *Phase structure of 2+1-flavor QCD from an Einstein-dilaton-flavor holographic model*, [2511.19127](#).
- [54] F. Becattini, M. Buzzegoli, T. Niida, S. Pu, A.-H. Tang and Q. Wang, *Spin polarization in relativistic heavy-ion collisions*, *Int. J. Mod. Phys. E* **33** (2024) 2430006 [[2402.04540](#)].
- [55] F. Becattini and C. Hoyos, *Pseudo-gauge invariant non-equilibrium density operator*, [2507.09249](#).
- [56] E. Witten, *Baryons and branes in anti-de Sitter space*, *JHEP* **07** (1998) 006 [[hep-th/9805112](#)].
- [57] M. Järvinen, E. Kiritsis, F. Nitti and E. Préau, *Tachyon-dependent Chern-Simons terms and the V-QCD baryon*, *JHEP* **12** (2022) 160 [[2209.05868](#)].
- [58] T. Alho, M. Järvinen, K. Kajantie, E. Kiritsis and K. Tuominen, *On finite-temperature holographic QCD in the Veneziano limit*, *JHEP* **01** (2013) 093 [[1210.4516](#)].